Journal of Catalysis 279 (2011) 123–135

Contents lists available at ScienceDirect

Journal of Catalysis

journal homepage: www.elsevier.com/locate/jcat

Photocatalytic conversion of carbon dioxide into methanol using zinc–copper–M(III) (M = aluminum, gallium) layered double hydroxides

Naveed Ahmed [a], Yoshiyuki Shibata [a], Tatsuo Taniguchi [b], Yasuo Izumi [a,*]

[a] Department of Chemistry, Graduate School of Science, Chiba University, Yayoi 1-33, Inage-ku, Chiba 263-8522, Japan
[b] Department of Applied Chemistry and Biotechnology, Graduate School of Engineering, Chiba University, Yayoi 1-33, Inage-ku, Chiba 263-8522, Japan

ARTICLE INFO

Article history:
Received 6 October 2010
Revised 7 January 2011
Accepted 9 January 2011
Available online 15 February 2011

Keywords:
CO_2
Photoreduction
Methanol
Layered double hydroxide
Copper

ABSTRACT

Ordered layered double hydroxides (LDHs) consisting of zinc and/or copper hydroxides were synthesized and combined with aluminum or gallium. These LDH compounds were then applied as photocatalysts to convert gaseous CO_2 (2.3 kPa) to methanol or CO under UV–visible light using hydrogen. Zn—Al LDH was the most active for CO_2 photoreduction and the major product was CO formed at a rate of 620 nmol h^{-1} g_{cat}^{-1}, whereas methanol was the major product formed by the inclusion of Cu in the LDH photocatalysts, e.g., at a formation rate of 170 nmol h^{-1} g_{cat}^{-1} using Zn—Cu—Ga photocatalyst. The methanol selectivity improved by the inclusion of Cu from 5.9 to 26 mol% and 39 to 68 mol%, respectively, when Zn—Al (the conversion 0.16–0.11%) and Zn—Ga LDH catalysts were used (the conversion 0.02–0.03%). Specific interaction of Cu sites with CO_2 was spectroscopically suggested to enable coupling with protons and photogenerated electrons to form methanol.

1. Introduction

Carbon dioxide is one of the major greenhouse gases [1]. Several methods for reducing CO_2 concentration in the atmosphere have been investigated, such as increasing green carbon sinks (plants, phytoplankton, and algae containing chloroplasts); increasing dissolved carbonate and its salts in sea water; or capturing CO_2 and transferring it to the bottom of the sea in a supercritical state. It would be advantageous to capture CO_2 from the atmosphere and convert it to fuels using sustainable energy such as sunlight, because this solves the problems of global warming and sustainable energy shortage simultaneously.

The major obstacle to realizing this option is the thermodynamic limitation on the chemical conversion:

$$CO_2(g) + 2H_2O(g) \rightarrow CH_3OH(g) + 1.5O_2(g), \quad \Delta G_r^\circ = +689\ \text{kJ mol}^{-1}.$$

Since an efficient catalyst for this photoconversion to fuel is unknown [2–12], it is also important to investigate good catalysts for CO_2 conversion to methanol or other fuels using hydrogen as a reductant, which is potentially obtained from water splitting:

$$2H_2O(g) \rightarrow 2H_2(g) + O_2(g), \quad \Delta G_r^\circ = +457.2\ \text{kJ mol}^{-1}.$$

$$CO_2(g) + 3H_2(g) \rightarrow CH_3OH(g) + H_2O(g), \quad \Delta G_r^\circ = +2.9\ \text{kJ mol}^{-1}.$$

The latter reaction, using hydrogen, does not essentially solve the problems of global warming and sustainable energy shortage, because current hydrogen production processes require energy and produce CO_2. The hydrogen needs to be produced from water driven by sunlight if the photoreduction in this paper is to be utilized in a future environmentally benign society [13].

Catalysts for converting CO_2 to methanol using hydrogen at room temperature and utilizing UV–visible light were investigated in this study. As described above, this option requires technologies both to capture CO_2 from the atmosphere and to convert it into fuel. To satisfy the two requisites, layered double hydroxides (LDHs) were chosen with the expectation of (1) sorption capacity for CO_2 in the layered space and (2) tunable semiconductor properties (photocatalytically active) as a result of the choice of metal cations. LDHs are materials based on the layered structure of brucite ($Mg(OH)_2$), which has a hexagonal crystal structure, whereas the MgO_6 octahedra are linked at the edge to form sheets (Scheme 1A). One of the naturally occurring LDH compounds is hydrotalcite [14]. The charge of cationic sheets formulated as $[M^{II}_{1-x}M^{III}_x(OH)_2]^{x+}$ is compensated for by an intercalated anion group, e.g., CO_3^{2-}, SO_4^{2-}, NO_3^-, Cl^-, or OH^-, and the M^{II} site can be Mg, Mn, Fe, Co, Ni, Cu, or Zn. The M^{III} site can be Al, Cr, Mn, Fe, or Ga. x is normally variable within the range 0.17–0.33. The molar amount of structural water intercalated between the cationic layers is about half of the total molar amount of metal cations (Scheme 1A) [15–19].

As for the first requisite, the sorption capacity of LDHs was 0.5—1.4 mmol $g_{sorbent}^{-1}$, which was comparable to that of zeolites (0.95—3.2 mmol $g_{sorbent}^{-1}$) [20,21] and greater than that of

* Corresponding author. Fax: +81 43 290 2783.
E-mail address: yizumi@faculty.chiba-u.jp (Y. Izumi).

0021-9517/$ - see front matter © 2011 Elsevier Inc. All rights reserved.
doi:10.1016/j.jcat.2011.01.004

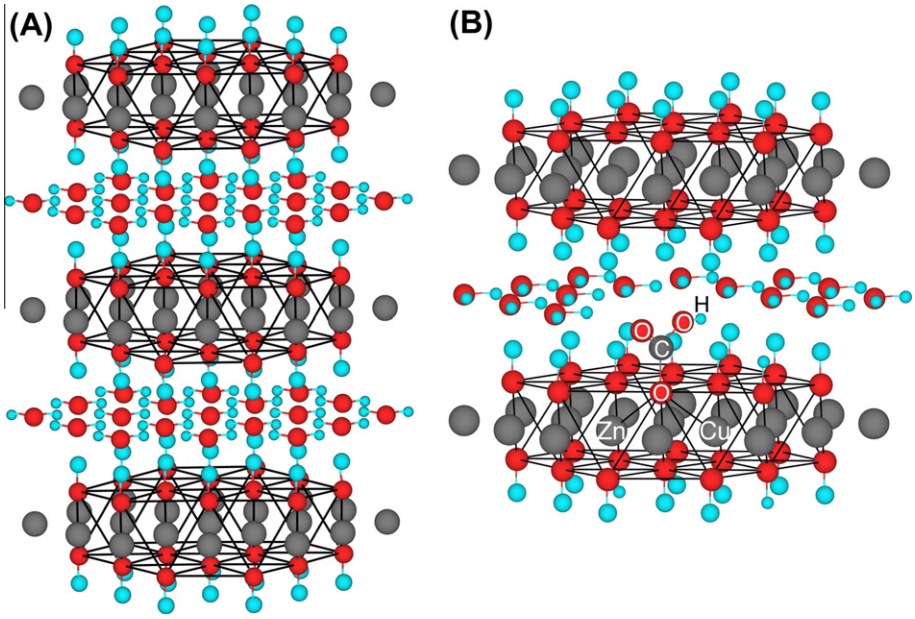

Scheme 1. (A) Structure of $Zn_{57-x-y}Cu_xM^{III}_y(OH)_{72} \cdot 38H_2O$ cluster models: (i) $x = y = 0$; (ii) $x = 0$, $y = 12$, M = Al; (iii) $x = 0$, $y = 1$, M = Ga; (iv) $x = 1$, $y = 0$; and (v) $x = 1$, $y = 12$, M = Al. (B) Hydrogen carbonate species formed from the reaction of CO_2 with the surface hydroxy group of $Zn_{57-x-y}Cu_xM^{III}_y(OH)_{72} \cdot 38H_2O$.

montmorillonites (0.4—0.5 mmol $g^{-1}_{sorbent}$) [22,23]. The proportion of carbonate ions in $[Zn_{0.75}Ga_{0.25}(OH)_2]^{0.25+}(CO_3)^{2-}_{0.125} \cdot mH_2O$ is 1.1 mmol g^{-1}_{LDH}. The tests for CO_2 sorption were reported for previously degassed LDH compounds in which the M^{II} site was Mg, Co, Ni, Cu, and Zn and the M^{III} site was Al and Ga [15,24–26]. In contrast to the fact that various negatively charged sheet layered materials such as montmorillonites, smectites, and kaolinites have been studied in detail, the number of positively charged sheet layered materials that can be applied directly to carbonate anion exchange is limited and they are not well studied.

As for the second requisite, Zn^{II} and Ga^{III} were chosen as the cations of LDHs to form the semiconductor samples. Zinc and copper have an affinity for CO_2 and they form carbonate and formate species in methanol synthesis, typically at 523–573 K [27]. In addition, Zn and Cu are associated with the trivalent elements Ga, Al, or Cr in the synthesis of industrial methanol [28]. In this context, LDH compounds $[Zn^{II}_{1-x-y}Cu^{II}_yM^{III}_x(OH)_2]^{x+}_{2/x}(CO_3)^{2-}$ consisting of Zn and/or Cu associated with Ga^{III} or Al^{III} were chosen to behave as semiconductors and potentially produce methanol via a photo process.

Photoreduction of CO_2 using hydrogen as a reductant has been reported to produce carbon monoxide using Rh/TiO_2 (5.1 μmol h^{-1} g^{-1}_{cat}) [29], ZrO_2 (0.51—0.70 μmol h^{-1} g^{-1}_{cat}) [30,31], MgO (1.6 μmol h^{-1} g^{-1}_{cat}) [32], and β-Ga_2O_3 (0.76 μmol h^{-1} g^{-1}_{cat}) [33], and to produce methane using TiO_2 (0.30 μmol h^{-1} g^{-1}_{cat}) [8,34]. In this study, new catalysts for producing methanol were found for the first time in the photoreaction of CO_2 using hydrogen as a reductant. The synthesis, photocatalytic performance, and spectroscopic monitoring of the interaction of metal sites with CO_2, and bandgap energies vs each reaction step of CO_2 reduction and that of H_2 oxidation to H^+ were reported.

2. Experimental

2.1. Syntheses

For the synthesis of LDH compounds, zinc nitrate hexahydrate (Wako Pure Chemical, >99%), copper nitrate trihydrate (Wako Pure Chemical, >99%), gallium nitrate hydrate (Wako Pure Chemical, >99.9%; n = 7–9 of $Ga(NO_3)_3 \cdot nH_2O$), aluminum nitrate nonahydrate (Wako Pure Chemical, >99.9%), sodium carbonate (Wako Pure Chemical, >99.8%), and sodium hydroxide (Kanto Chemical, >97.0%) were used as received. Deionized water (<1.0 μS cm^{-1}) was used throughout the syntheses.

An LDH compound formulated as $[Zn_3Ga^{III}(OH)_8]^+_2(CO_3)^{2-} \cdot mH_2O$ was synthesized [35]. A mixed solution (20 ml) of 0.75 M $Zn(NO_3)_2 \cdot 6H_2O$ and 0.25 M $Ga(NO_3)_3 \cdot nH_2O$ was dropped at a rate of 0.6 ml min^{-1} into 100 ml of a 0.075 M Na_2CO_3 solution in a flask at 290 K with stirring at a rate of 900 rpm. The pH was adjusted to 8 by adding 1.0 M NaOH (~20 ml total). After the addition was complete, the mixture was continuously stirred at the same rate at 290 K for 2 h. The pH was maintained at 8 by adding 1.0 M NaOH (~0.5 ml total). Then the temperature of the mixture was raised to 353 K and continuously stirred for an additional 22 h. The pH of the solution did not change from 8 throughout the 22 h. The obtained precipitates were filtered using a polytetrafluoroethene-based membrane filter (Omnipore JGWP04700, Millipore) with a pore size of 0.2 μm, washed with deionized water, and dried in ambient air at 290 K for 5 days. Following the same procedure, an LDH compound formulated as $[Zn_3Al^{III}(OH)_8]^+_2(CO_3)^{2-} \cdot mH_2O$ was synthesized using $Al(NO_3)_3 \cdot 9H_2O$ (0.25 M) instead of $Ga(NO_3)_3 \cdot nH_2O$ (0.25 M).

Cu atoms were substituted at the Zn^{II} sites in the LDH compounds formulated as $[Zn_3M^{III}(OH)_8]^+_2(CO_3)^{2-} \cdot mH_2O$ (M = Ga or Al). At the beginning of the synthesis, a mixed solution (20 ml) was prepared as 0.375 M $Zn(NO_3)_2 \cdot 6H_2O$, 0.375 M $Cu(NO_3)_2 \cdot 3H_2O$, and 0.25 M $Al(NO_3)_3 \cdot 9H_2O$ (or 0.25 M $Ga(NO_3)_3 \cdot nH_2O$) to set the molar ratio of Zn^{II}, Cu^{II}, and M^{III} (Ga, Al) ions to 3:3:2. Henceforth, the steps are essentially identical to those described above for the syntheses of $[Zn_3M^{III}(OH)_8]^+_2(CO_3)^{2-} \cdot mH_2O$.

2.2. Characterization

Nitrogen adsorption isotherm measurements were performed at 77 K within the pressure range 1.0–90 kPa in a vacuum system connected to diffusion and rotary pumps (10^{-6} Pa) and equipped with a capacitance manometer (Models CCMT-1000A and GM-2001, ULVAC). The Brunauer–Emmett–Teller (BET) surface area (S_{BET}) was calculated on the basis of eight-point measurements

between 10 and 46 kPa (P/P_0 = 0.10–0.45) on the adsorption isotherm. The samples were evacuated at 383 K for 2 h before the measurements.

X-ray diffraction (XRD) data were obtained using a MiniFlex diffractometer (Rigaku) at a Bragg angle of $2\theta_B$ = 5–70° with a scan step of 0.01° and a scan rate of 7 s per step for the sample powders. The measurements were performed at 30 kV and 15 mA using Cu Kα emission and a nickel filter. Scanning electron microscopy (SEM) measurements were performed using JEOL Model JSM-6510A at the Chemical Analysis Center, Chiba University. The samples were mounted on a conducting carbon tape and coated with gold. The electron accelerating voltage was between 15 and 25 kV and the magnification was between 20,000 and 50,000 times.

Optical spectroscopic measurements were performed using a UV–visible spectrophotometer (JASCO, Model V-650). D_2 and halogen lamps for wavelengths below and above 340 nm, respectively, and an integrating sphere (JASCO, Model ISV-469) were used for the diffuse reflectance measurements. Measurements were performed at 290 K within the wavelength range 200–900 nm using 100 mg of fresh samples. Diffuse reflectance spectra were converted to absorption spectra on the basis of the Kubelka–Munk equation [36,37]. The bandgap value was evaluated on the basis of either simple extrapolation of the absorption edge or the fit to the equation of Davis and Mott [37],

$$\alpha \times h\nu \propto (h\nu - E_g)^n,$$

in which α, h, and ν are the absorption coefficient, Planck's constant, and the wavenumber, respectively, and n is 1/2, 3/2, 2, and 3 for allowed direct, forbidden direct, allowed indirect, and forbidden indirect transitions, respectively.

Cu, Zn, and Ga K-edge X-ray absorption fine structure (XAFS) spectra were measured at 30–290 K in transmission mode in the Photon Factory at the High Energy Accelerator Research Organization (Tsukuba) on beamlines 7C and 9C. The storage-ring energy was 2.5 GeV and the top-up ring current was 450 mA. A Si(1 1 1) double-crystal monochromator was inserted into the X-ray beam path. The X-ray intensity was maintained at 65% of the maximum flux using a piezo translator set to the crystal. The slit opening size was 1 mm (vertical) × (1–3) mm (horizontal) in front of the I_0 ionization chamber. The I_0 and $I_{transmit}$ ionization chambers were purged with N_2 and Ar, respectively. The scan steps were ~9, ~0.3, and ~2.5 eV in the pre-edge, edge, and postedge regions, respectively. The data accumulation time was 1–5 s for each data point. The Zn K, Cu K, and Ga K-edge absorption energy values were calibrated to 9660.7, 8980.3, and 10,368.2 eV for the spectra of Zn, Cu, and Ga metals, respectively [38,39]. The energy position of the monochromator was reproduced within ±0.1 eV.

2.3. Analyses

The XAFS data were analyzed using an XDAP package [40]. The pre-edge background was approximated by a modified Victoreen function, $C_2/E^2 + C_1/E + C_0$. The background of the postedge oscillation was approximated by a smoothing spline function, calculated by an equation for the number of data points, where k is the wavenumber of photoelectrons:

$$\sum_{i=1}^{\text{Data Points}} \frac{(\mu x_i - BG_i)^2}{\exp(-0.075k_i^2)} \leqslant \text{smoothing factor}.$$

Multiple-shell curve-fit analyses were performed for the Fourier-filtered k^3-weighted extended X-ray absorption fine structure (EXAFS) data in k- and R-space using empirical amplitude and phase-shift parameters extracted from the EXAFS data for CuO and ZnO. The interatomic distance (R) and its associated coordination number (N) for the Cu—O and Zn—O pairs were set to 0.19521 nm with the N value of 4 [41] and to 0.1978 nm with the N value of 4, respectively, on the basis of their crystal structure [42]. The many-body reduction factor S_0^2 was assumed to be equal for the sample and the reference.

The amplitude and phase-shift parameters were also generated theoretically for Zn···Zn (R = 0.308 nm with an N value of 6), Zn···Zn (R = 0.53347 nm with an N value of 6), and Zn···Zn pairs (R = 0.616 nm with an N value of 6) using a $Zn_{57}(OH)_{72}$ model (Scheme 1A-i), and for the Zn···Al pair (R = 0.308 nm with an N value of 2) using a $Zn_{45}Al_{12}(OH)_{72}$ model (Scheme 1A-ii) using the ab initio calculation code FEFF 8.4 [43] in the self-consistent field mode. One-fourth of the Zn sites were periodically replaced by Al atoms in the $Zn_{45}Al_{12}(OH)_{72}$ model. The exchange–correlation potential of Hedin–Lundqvist was chosen. The Debye temperature of the LDH models was assumed to be equal to that of ZnO (370 K) [44]. The goodness of fit was given as requested by the Committee on Standards and Criteria in X-ray Absorption Spectroscopy.

The Zn, Cu, and Ga K-edge X-ray absorption near-edge structure (XANES) spectra were theoretically generated using FEFF 8.4 operated in the self-consistent field mode and the fully multiple scattering mode.

2.4. Photocatalytic reduction of CO_2

Photocatalytic reactions were conducted in a closed circulating system using a photoreaction cell with a flat quartz bottom (total volume of reaction system 186 ml, Fig. S1) [45]. One hundred milligrams of the LDH catalyst was homogenously spread in a quartz reaction cell (bottom plate area 23.8 cm^2) connected to the circulation loop and evacuated (10^{-6} Pa) at 290 K for 2 h as pretreatment until the desorbed gas was detected by an online gas chromatograph (GC). Either 21.7 kPa of H_2 (1.67 mmol) or 2.3 kPa of CO_2 (0.177 mmol) + 21.7 kPa of H_2 (1.67 mmol) was introduced and allowed to circulate for 30 min in contact with the catalyst to reach a sorption equilibrium before the photoillumination.

The catalyst was then illuminated with UV–visible light obtained from a 500-W xenon arc lamp (Ushio, Model UI-502Q) through the flat bottom of the quartz reactor (Fig. S1A) for 5 h. The distance between the bottom of the reactor and the lamp exit window was set to 20 mm. The light intensity at the wavelength of 555 nm was 42 mW cm^{-2} at the center of the sample cell and 28 mW cm^{-2} at the periphery of the bottom plate of the sample cell. Note that the intensity was measured at 555 nm but the Xe arc lamp irradiated in a wide spectrum between 200 and 1100 nm. The temperature was within the range 305–313 K at the catalyst position during the illumination (Fig. S2). The transmitted light intensity was also evaluated by changing the catalyst amount between 0 and 0.2 g (Fig. S3). Half of the incident light was absorbed or scattered by 0.1 g of catalyst charged and half was transmitted. Because the transmitted light intensity monotonically decreased as the catalyst amount increased, most of 0.1 g of catalyst should have been effectively illuminated. As a comparison, one of the LDH catalysts was illuminated with UV–visible light obtained from another 500-W xenon arc lamp (Ushio, Model SX-UID502XAM) through a UV hot mirror (3.3 mm thick; Edmond), a water filter (100-mm thickness), and the flat bottom of the quartz reactor (Fig. S1B). The distance between the bottom of the reactor and the lamp exit window was set to 206 mm. The light intensity at 555 nm was 106 mW cm^{-2} at the maximum of the sample cell and 76 mW cm^{-2} at the periphery of the bottom plate of the sample cell.

To evaluate the dependence of the photocatalytic reaction rates on wavelength, a sharp cutoff filter, UV-32 (>320 nm), L-37 (>370 nm), L-42 (>420 nm), or Y-48 (>480 nm) (Kenko), was set at the lamp exit window [45]. The liquid nitrogen trap was used

Table 1
Physicochemical characterization of $[Zn_{3-x}Cu_xM^{III}(OH)_8]_2^+(CO_3)^{2-}\cdot mH_2O$ (x = 0, 1.5; M^{III} = Al, Ga) layered double hydroxides and reference catalysts.

Sample	S_{BET} ($m^2\ g^{-1}$)	E_g (eV)					Interlattice distance (nm)	
		Extrapolated	Fit to $\alpha \times h\nu \propto (h\nu - E_g)^n$, n =					
			1/2	3/2	2	3	(0 0 3)	(1 1 0)
(A) $Zn_{3-x}Cu_xAl^{III}$LDHs								
$[Zn_3Al(OH)_8]_2^+(CO_3)^{2-}\cdot mH_2O$	57	5.7	5.9	5.5	5.3	5.0	0.757	0.154
$[Zn_{1.5}Cu_{1.5}Al(OH)_8]_2^+(CO_3)^{2-}\cdot mH_2O$	38	4.1	4.5	3.8	3.4	2.7	0.753	0.154
(B) $Zn_{3-x}Cu_xGa^{III}$ LDHs								
$[Zn_3Ga(OH)_8]_2^+(CO_3)^{2-}\cdot mH_2O$	70	5.6	5.9	5.4	5.2	5.0	0.751	0.155
$[Zn_{1.5}Cu_{1.5}Ga(OH)_8]_2^+(CO_3)^{2-}\cdot mH_2O$	57	3.5	4.2	3.2	3.0	2.6	0.753	0.155
(C) References								
Cu—ZnO[a]	41							
Ga_2O_3[b]	2.0							

[a] The Cu—ZnO catalyst was prepared via the reported inverse precipitation method starting from copper and zinc nitrates (atomic ratio Cu:Zn = 54:46) with $NaHCO_3$ [27].
[b] Commercial sample (Kanto Chemical, 99.0%). The major crystalline phase was α-Ga_2O_3.

for the reaction in H_2 gas only to condense the formed CO_2, CH_3OH, and H_2O. Products and reactants were analyzed using packed columns of Molecular Sieve 13X-S and PEG (polyethylene glycol)-6000 supported on Flusin P (GL Sciences) set in the online GC equipped with a thermal conductivity detector (Shimadzu, Model GC-8A). Two blank tests were performed: a reaction test illuminated with UV–visible light in the absence of photocatalysts and another test for catalyst in the absence of any light. For the latter test, the reactor was completely wrapped with 20-μm-thick aluminum foil. To confirm the photocatalytic methanol synthesis, reactivity tests on carbonates in LDHs in H_2 gas and photocatalytic tests on LDHs in CO_2 gas were also performed. Furthermore, the change in the photocatalytic performance when the gas was switched to a mixture of $CO_2 + H_2$ was investigated.

3. Results

3.1. Nitrogen adsorption, XRD, SEM, and UV–visible spectra

The S_{BET} value was measured on the basis of the N_2 adsorption at 77 K for LDH compounds preheated at 383 K (Table 1). The S_{BET} value for $[Zn_3Ga(OH)_8]_2^+(CO_3)^{2-}\cdot mH_2O$ (70 $m^2\ g^{-1}$) was 21% greater than that for $[Zn_3Al(OH)_8]_2^+(CO_3)^{2-}\cdot mH_2O$. The S_{BET} value decreased by 19% for $[Zn_3Ga(OH)_8]_2^+(CO_3)^{2-}\cdot mH_2O$ and by 34% for $[Zn_3Al(OH)_8]_2^+(CO_3)^{2-}\cdot mH_2O$ by substitution of Cu atoms at half of the Zn sites.

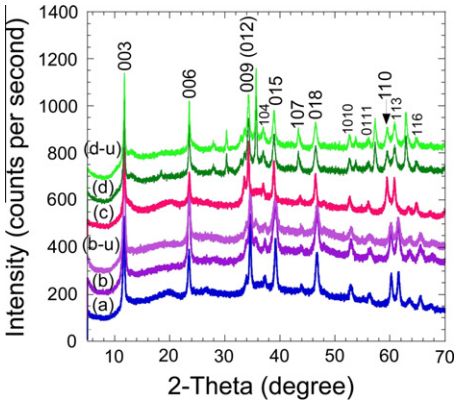

Fig. 1. XRD spectra of fresh samples of $[Zn_3Al(OH)_8]_2^+(CO_3)^{2-}\cdot mH_2O$ (a), $[Zn_{1.5}Cu_{1.5}Al(OH)_8]_2^+(CO_3)^{2-}\cdot mH_2O$ (b), $[Zn_3Ga(OH)_8]_2^+(CO_3)^{2-}\cdot mH_2O$ (c), and $[Zn_{1.5}Cu_{1.5}Ga(OH)_8]_2^+(CO_3)^{2-}\cdot mH_2O$ (d) and the used samples of $[Zn_{1.5}Cu_{1.5}Al(OH)_8]_2^+(CO_3)^{2-}\cdot mH_2O$ (b-u) and $[Zn_{1.5}Cu_{1.5}Ga(OH)_8]_2^+(CO_3)^{2-}\cdot mH_2O$ (d-u) in 2.3 kPa of CO_2 + 21.7 kPa of H_2 under UV–visible light for 5 h.

The XRD spectra measured for $[Zn_3Al(OH)_8]_2^+(CO_3)^{2-}\cdot mH_2O$ and $[Zn_{1.5}Cu_{1.5}Al(OH)_8]_2^+(CO_3)^{2-}\cdot mH_2O$ are depicted in Fig. 1a and b. The diffraction peaks common at $2\theta_B$ = 11.7°, 23.5°, 34.6°, 37.3°, 39.2°, 43.9°, 46.7°, 52.9°, 56.3°, 60.2°, 61.5°, and 65.5° were assigned to (0 0 3), (0 0 6), (0 0 9), (1 0 4), (0 1 5), (1 0 7), (0 1 8), (1 0 10), (0 1 11), (1 1 0), (1 1 3), and (1 1 6) diffraction for the regular layered structure, respectively [46,47]. The interlayer interval was evaluated as 0.757 and 0.753 nm on the basis of the (0 0 3) diffraction angle (Table 1A), consistent with the values 0.757 and 0.756 nm, which were evaluated based on the (0 0 6) diffraction angle. The interlayer interval value was 0.777 nm, on the basis of the (0 0 9) diffraction. The small difference may be due to the overlap of the diffraction peak (0 0 9) with the (0 1 2) diffraction. The in-plane (1 1 0) diffraction angle (0.154 nm, Table 1A) within a layer corresponds to R(Zn—O) of 0.218 nm if complete ZnO_6 octahedra are assumed. Compared to the R(Zn—O) values provided by the Zn K-edge EXAFS analyses for $[Zn_3Al(OH)_8]_2^+(CO_3)^{2-}\cdot mH_2O$ and $[Zn_{1.5}Cu_{1.5}Al(OH)_8]_2^+(CO_3)^{2-}\cdot mH_2O$ (0.205–0.207 nm), the LDH cation sheets were found to be slightly elongated in the direction of the cationic layer plane.

The $2\theta_B$ angles of plane-to-plane diffraction peaks (0 0 3), (0 0 6), and (0 0 9) perpendicular to the cationic layers changed negligibly when Ga atoms were substituted at the trivalent Al sites (Fig. 1c and d). In contrast, other peaks significantly shifted toward smaller angles, reflecting the greater ionic radius of Ga^{III} than of Al^{III}, e.g., $2\theta_B$ for (1 1 0) diffraction of 60.2° (0.154 nm) for Al-containing LDHs to 59.5° (0.155 nm) for Ga-containing LDHs (Table 1). In the spectrum d for $Zn_{1.5}Cu_{1.5}Ga(OH)_8]_2^+(CO_3)^{2-}\cdot mH_2O$, peaks at $2\theta_B$ = 27.9°, 30.3°, 35.7°, 57.3°, and 62.9° were also observed, which were derived from the impurity.

A representative SEM image for $[Zn_3Al(OH)_8]_2^+(CO_3)^{2-}\cdot mH_2O$ is depicted in Fig. 2. Flat flakes smaller than 100 nm were observed, which suggested the coagulation of the stacked layered structure.

As indicated in Fig. 1b-u and d-u, the LDH samples after the photocatalytic tests in 2.3 kPa of CO_2 + 21.7 kPa of H_2 under UV–visible light for 5 h differed negligibly from the corresponding data for fresh samples (Fig. 1b and d); therefore, the layered structures of as-synthesized $Zn_{1.5}Cu_{1.5}Al(OH)_8]_2^+(CO_3)^{2-}\cdot mH_2O$ and $Zn_{1.5}Cu_{1.5}Ga(OH)_8]_2^+(CO_3)^{2-}\cdot mH_2O$ samples should be well retained.

An extrapolation of the absorption edge in the UV–visible absorption spectra was drawn (Fig. 3A). The intercepts with the x-axis for $[Zn_3Al(OH)_8]_2^+(CO_3)^{2-}\cdot mH_2O$ and $[Zn_3Ga(OH)_8]_2^+(CO_3)^{2-}\cdot mH_2O$ were 218 and 222 nm, respectively (Spectra a, c), corresponding to bandgap values of 5.7 for $[Zn_3Al(OH)_8]_2^+(CO_3)^{2-}\cdot mH_2O$ and 5.6 eV for $[Zn_3Ga(OH)_8]_2^+(CO_3)^{2-}\cdot mH_2O$ (Table 1). The bandgap values based on the fit to the equation of Davis and

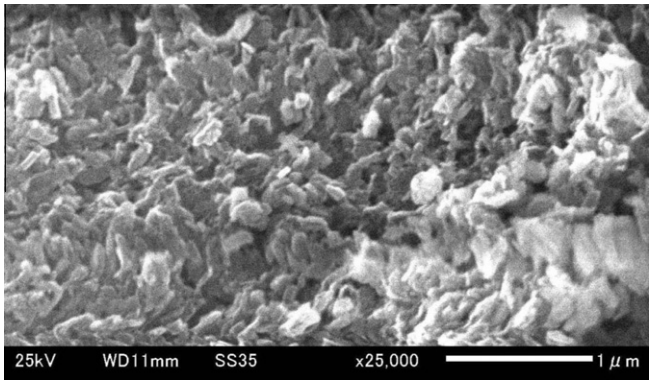

Fig. 2. SEM image for $[Zn_3Al(OH)_8]_2^+(CO_3)^{2-} \cdot mH_2O$.

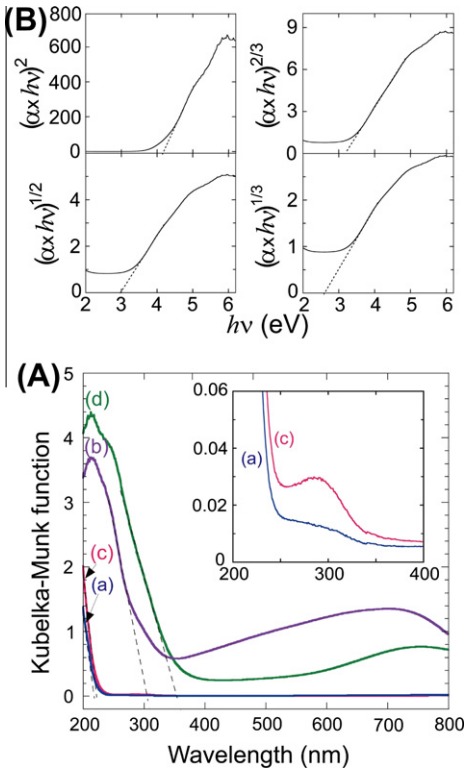

Fig. 3. (A) Diffuse reflectance UV–visible absorption spectra of fresh samples of $[Zn_3Al(OH)_8]_2^+(CO_3)^{2-} \cdot mH_2O$ (a), $[Zn_{1.5}Cu_{1.5}Al(OH)_8]_2^+(CO_3)^{2-} \cdot mH_2O$ (b), $[Zn_3Ga(OH)_8]_2^+(CO_3)^{2-} \cdot mH_2O$ (c), and $[Zn_{1.5}Cu_{1.5}Ga(OH)_8]_2^+(CO_3)^{2-} \cdot mH_2O$ (d). (Inset) Expanded spectra (a) and (c). (B) Fit to the equation of Davis and Mott ($\alpha \times h\nu \propto (h\nu - E_g)^n$) for data of spectrum (d). $(\alpha \times h\nu)^2$, $(\alpha \times h\nu)^{2/3}$, $(\alpha \times h\nu)^{1/2}$, or $(\alpha \times h\nu)^{1/3}$ vs $h\nu$ was plotted and the intercept with the x-axis estimates the E_g value.

Mott by applying different n values were within the range 5.0–5.9 eV both for $[Zn_3Al(OH)_8]_2^+(CO_3)^{2-} \cdot mH_2O$ and for $[Zn_3Ga(OH)_8]_2^+(CO_3)^{2-} \cdot mH_2O$. The bandgap values in the case of $n = 1/2$ or $3/2$ were relatively similar to the corresponding bandgap values based on simple absorption edge extrapolation (Table 1). The electronic transition for $[Zn_3M^{III}(OH)_8]_2^+(CO_3)^{2-} \cdot mH_2O$ could be a direct process from oxygen 2p to metal ns or np levels ($n = 4$ for Zn and Ga and $n = 3$ for Al). In addition, a weak peak was observed centered at 291 nm for $[Zn_3Ga(OH)_8]_2^+(CO_3)^{2-} \cdot mH_2O$ and a weaker peak was observed for $[Zn_3Al(OH)_8]_2^+(CO_3)^{2-} \cdot mH_2O$ (Fig. 3A, insets c, a).

By the inclusion of Cu, the UV absorption edge shifted toward the lower-energy side for $[Zn_{1.5}Cu_{1.5}Al(OH)_8]_2^+(CO_3)^2 \cdot mH_2O$ (Fig. 3A-b) and shifted to further lower energy for $[Zn_{1.5}Cu_{1.5}Ga(OH)_8]_2^+(CO_3)^{2-} \cdot mH_2O$ (Spectrum d). The extrapolation of the absorption edge was drawn and the intercepts with the x-axis for $[Zn_{1.5}Cu_{1.5}Al(OH)_8]_2^+(CO_3)^{2-}H_2O$ and $[Zn_{1.5}Cu_{1.5}Ga(OH)_8]_2^+(CO_3)^{2-}H_2O$ were 306 and 354 nm, respectively, corresponding to the bandgap values of 4.1 for $[Zn_{1.5}Cu_{1.5}Al(OH)_8]_2^+(CO_3)^{2-} \cdot mH_2O$ and 3.5 eV for $[Zn_{1.5}Cu_{1.5}Ga(OH)_8]_2^+(CO_3)^{2-} \cdot mH_2O$ (Table 1). The bandgap values calculated on the basis of the fit to the Davis and Mott equation by applying different n values were 2.7–4.5 for $[Zn_{1.5}Cu_{1.5}Al(OH)_8]_2^+(CO_3)^{2-} \cdot mH_2O$ and 2.6–4.2 eV for $[Zn_{1.5}Cu_{1.5}Ga(OH)_8]_2^+(CO_3)^{2-} \cdot mH_2O$ (Table 1 and Fig. 3B). The bandgap values in the case of $n = 3/2$ were similar to the corresponding bandgap values based on simple extrapolation. The electronic transition for $[Zn_{1.5}Cu_{1.5}M^{III}(OH)_8]_2^+(CO_3)^{2-} \cdot mH_2O$ might be a forbidden direct process from oxygen 2p to metal ns or np levels ($n = 4$ for Cu, Zn, and Ga and $n = 3$ for Al).

3.2. XANES spectra for fresh $[Zn_{3-x}Cu_xX(OH)_8]_2^+(CO_3)^{2-} \cdot mH_2O$

Zn K-edge XANES spectra for LDH samples in comparison to the reference spectra are shown in Fig. 4A. The entire spectral patterns for $[Zn_3Al(OH)_8]_2^+(CO_3)^{2-} \cdot mH_2O$ and $[Zn_{1.5}Cu_{1.5}Al(OH)_8]_2^+(CO_3)^{2-} \cdot mH_2O$ (Spectra b and c) closely resemble each other. In both spectra, an intense peak at 9671.7 eV is accompanied by weak, broad peaks at 9688, 9715, and 9724 eV. The Cu K-edge XANES pattern for the latter sample closely resembles those of the corresponding Zn K-edge data (Fig. 4A-c and B-c), strongly suggesting an identical coordination environment for Cu and Zn in $[Zn_{1.5}Cu_{1.5}Al(OH)_8]_2^+(CO_3)^{2-} \cdot mH_2O$. The energy values of postedge peaks relative to the first intense peak were 16, 44, and 52 eV for the Cu K-edge, similar to the gaps of 16, 43, and 52 eV for the Zn K-edge.

The patterns of these experimental spectra were reproduced in the theoretically generated Zn K-edge spectrum for a complete octahedral model (Fig. 4A-f) and theoretically generated Cu K-edge spectrum for a complete octahedral model (Fig. 4B-h and Scheme 1A-v, ii). The energy values of the Zn K postedge peaks relative to the first intense peak were 16, 39, and 47 eV in the theoretical spectrum (Fig. 4A-f) compared to 16, 43, and 52 eV in the corresponding experimental spectrum (Fig. 4A-b). The energy values of the Cu K postedge peaks relative to the first intense peak were 14, 39, and 46 eV in the theoretical spectrum (Fig. 4B-h) compared to 16, 44, and 52 eV in the corresponding experimental spectrum (Fig. 4B-c). Thus, the Zn and Cu sites in $[Zn_3Al(OH)_8]_2^+(CO_3)^{2-} \cdot mH_2O$ and $[Zn_{1.5}Cu_{1.5}Al(OH)_8]_2^+(CO_3)^{2-} \cdot mH_2O$ should show nearly complete octahedral coordination.

The Zn K-edge XANES spectra for $[Zn_{3-x}Cu_xGa(OH)_8]_2^+(CO_3)^{2-} \cdot mH_2O$ ($x = 0, 1.5$) also consisted of intense peaks at 9671.7–9672.2 eV accompanied by weak, broad peaks at 9688–9689 eV (Fig. 4A, Spectra d and e), similar to spectra b and c for $[Zn_{3-x}Cu_xAl(OH)_8]_2^+(CO_3)^{2-} \cdot mH_2O$ ($x = 0, 1.5$). A minor difference was that weak, broad peaks at 9715 and 9724 eV observed for $[Zn_{3-x}Cu_xAl(OH)_8]_2^+(CO_3)^{2-} \cdot mH_2O$ merged into a weak, broad peak ranging from 9718 to 9720 eV for $[Zn_{3-x}Cu_xGa(OH)_8]_2^+(CO_3)^{2-} \cdot mH_2O$. The energy position of the experimental three peaks for $[Zn_{3-x}Cu_xGa(OH)_8]_2^+(CO_3)^{2-} \cdot mH_2O$ was reproduced in the theoretically generated Zn K-edge XANES spectrum for a complete octahedral model (Scheme 1A-i; Fig. 4A-g). Note that $_{30}$Zn, $_{29}$Cu, and $_{31}$Ga are similar photoelectron backscatters compared to the lighter element $_{13}$Al.

The Cu K-edge XANES spectrum for $[Zn_{1.5}Cu_{1.5}Ga(OH)_8]_2^+(CO_3)^{2-}H_2O$ closely resembled the corresponding Zn K-edge data (Fig. 4A-e and B-e). The energy values of the postedge peaks relative to the first intense peak were 17 and 48 eV for the Zn K-edge, identical to the gaps for the Cu K-edge. The energy position of the three experimental peaks in the Cu K-edge spectrum e for $[Zn_{1.5}Cu_{1.5}Ga(OH)_8]_2^+(CO_3)^{2-} \cdot mH_2O$ was closely reproduced in the

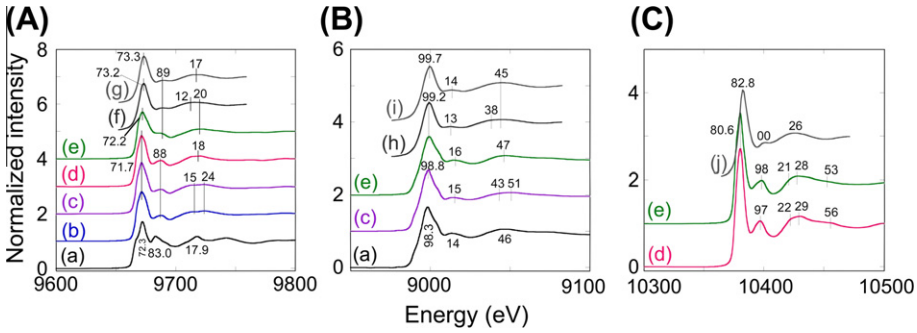

Fig. 4. (A) Normalized Zn, (B) Cu, and (C) Ga K-edge XANES spectra for ZnO (A-a), CuO (B-a), $[Zn_3Al(OH)_8]_2^+(CO_3)^{2-}\cdot mH_2O$ (b), $[Zn_{1.5}Cu_{1.5}Al(OH)_8]_2^+(CO_3)^{2-}\cdot mH_2O$ (c), $[Zn_3Ga(OH)_8]_2^+(CO_3)^{2-}\cdot mH_2O$ (d), and $[Zn_{1.5}Cu_{1.5}Ga(OH)_8]_2^+(CO_3)^{2-}\cdot mH_2O$ (e). Theoretical spectra generated using FEFF 8.4 for $Zn_{45}Al_{12}(OH)_{72}$ (f), $Zn_{57}(OH)_{72}$ (g), $CuZn_{44}Al_{12}(OH)_{72}$ (h), $CuZn_{56}(OH)_{72}$ (i), and $GaZn_{56}(OH)_{72}$ models (j). The central, X-ray absorbing atoms were Zn (f, g), Cu (h, i), and Ga (j).

theoretical Cu K-edge spectra for the complete octahedral model (Fig. 4B-i). Thus, as in the case of $[Zn_{3-x}Cu_xAl(OH)_8]_2^+(CO_3)^{2-}\cdot mH_2O$, the Zn and Cu sites show nearly complete octahedral coordination.

The Cu K-edge XANES pattern for CuO (Fig. 4B-a) was similar to those for $[Zn_{1.5}Cu_{1.5}Ga(OH)_8]_2^+(CO_3)^{2-}\cdot mH_2O$ (spectrum e) and the $CuZn_{56}(OH)_{72}$ model (spectrum i). The Cu sites in CuO are coordinated with four equatorial O atoms (average Cu—O distance 0.19521 nm) and two farther axial O atoms (average Cu—O distance 0.2817 nm). The Cu K-edge XANES pattern could be relatively insensitive to the variation in Cu—O distances [41].

The Ga K-edge XANES spectra for $[Zn_{3-x}Cu_xGa(OH)_8]_2^+(CO_3)^{2-}\cdot mH_2O$ ($x = 0$, 1.5) are depicted in Fig. 4C-d, e. The intense peak situated just above the edge (10,380.6 eV) and the three weak, broad postedge peaks appeared. The energy values of the postedge peaks relative to the first intense peak were 16–17, 40–41, and 47–48 eV, somewhat different from the gaps of 17 and 43 eV for the theoretically generated Ga K-edge spectrum for the complete octahedral model (Fig. 4C-j). A possible explanation for this discrepancy is that there is a significant distortion of Ga^{III} site coordination compared to the nearly complete octahedral ZnO_6 or CuO_6 coordination.

3.3. XANES spectra for partially dehydrated and CO_2-adsorbed $[Zn_{3-x}Cu_xX(OH)_8]_2^+(CO_3)^{2-}\cdot mH_2O$

When the $[Zn_{1.5}Cu_{1.5}Ga(OH)_8]_2^+(CO_3)^{2-}\cdot mH_2O$ sample was heated at 383 K for 1 h in vacuum, the intensity of the first postedge peak at 9689 eV in the Zn K-edge XANES for a fresh sample (Fig. 5A-e) decreased to 65% (Fig. 5A-e-383). In fact, the postedge peak intensity decreased to 58% when the theoretically generated XANES spectra for $Zn_{57}(OH)_{72}\cdot 38H_2O$ model (Scheme 1A-i and Fig. 5A-k) lost all the structural water (Fig. 5A-g). In contrast, a clear additional peak was not found in the Fourier transform of the theoretically generated Zn K-edge EXAFS besides those derived from the in-plane Zn—O, Zn···Zn ($R = 0.308$ nm), Zn···O ($R = 0.37722$ nm), Zn···Zn ($R = 0.53347$ nm), or Zn···Zn pair ($R = 0.616$ nm) on going from the spectrum for the $Zn_{57}(OH)_{72}$ model to the one for the $Zn_{57}(OH)_{72}\cdot 38H_2O$ model. When 34.3 kPa of CO_2 was introduced into the 383 K-heated LDH sample, the postedge peak intensity increased slightly to 72% of the fresh sample (Fig. 5A-e-CO_2-290). When the LDH sample was heated to 423 K in CO_2, the peak intensity further increased to 83% of spectrum e (spectrum e-CO_2-423, Table 2A). Note that the postedge peak is in the "multiple scattering" region, and the peak intensity increased in the presence of either water or CO_2 molecules between the LDH cationic layers.

A similar in situ trend was observed in the Cu K-edge XANES for the LDH compound of $[Zn_{1.5}Cu_{1.5}Ga(OH)_8]_2^+(CO_3)^{2-}\cdot mH_2O$. The intensity of the first postedge peak at 9016 eV decreased to 76% by heating in vacuum at 383 K (Fig. 5B-e → e-383). Upon introduction of CO_2, the peak intensity increased back to 87% of the fresh sample at 290 K (spectrum e-CO_2-290) and 91% of the fresh one at 423 K (spectrum e-CO_2-423, Table 2B).

It should be noted that these semireversible in situ peak intensity changes in both the Zn and Cu K-edges for

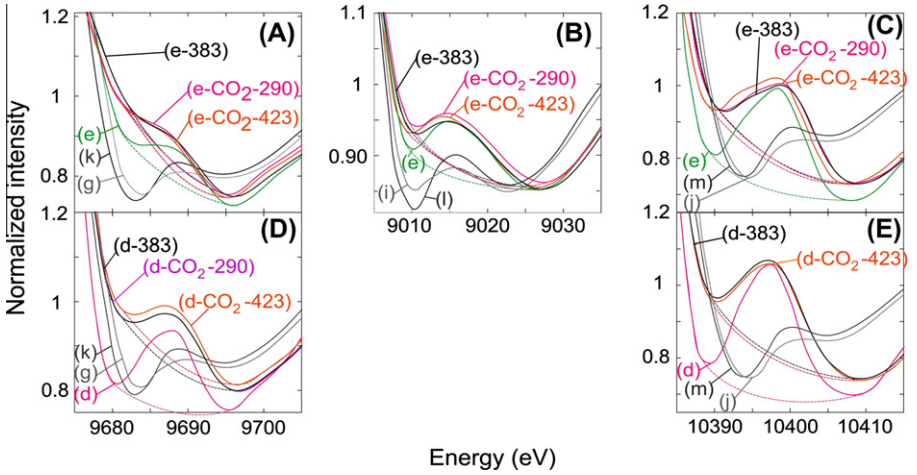

Fig. 5. Normalized Zn (A, D), Cu (B), and Ga K-edge XANES (C, E) spectra for $[Zn_{1.5}Cu_{1.5}Ga(OH)_8]_2^+(CO_3)^{2-}\cdot mH_2O$ (A–C) and $[Zn_3Ga(OH)_8]_2^+(CO_3)^{2-}\cdot mH_2O$ (D and E). As-synthesized (e), sample (e) in vacuum at 383 K (e-383), and sample (e-383) in 34.3 kPa of CO_2 at 290 K (e-CO_2-290) or 423 K (e-CO_2-423). Theoretical spectrum using FEFF 8.4 for $Zn_{57}(OH)_{72}$ (g), $CuZn_{56}(OH)_{72}$ (i), $GaZn_{56}(OH)_{72}$ (j), $Zn_{57}(OH)_{72}\cdot 38H_2O$ (k), $CuZn_{56}(OH)_{72}\cdot 38H_2O$ (l), and $GaZn_{56}(OH)_{72}\cdot 38H_2O$ (m). The central, X-ray absorbing atoms were Zn (g, k), Cu (i, l), and Ga (j, m).

Table 2
First postedge peak intensity in normalized Zn, Cu, and Ga K-edge XANES spectra.[a]

Sample	As-synthesized	In vacuum	In CO_2 (34.3 kPa)	
		383 K	290 K	423 K
(A) At Zn K-edge (9688–9689 eV)				
$[Zn_3Ga(OH)_8]_2^+(CO_3)^{2-}\cdot mH_2O$	0.19	0.12 (64%)	0.12 (64%)	0.12 (63%)
$[Zn_{1.5}Cu_{1.5}Ga(OH)_8]_2^+(CO_3)^{2-}\cdot mH_2O$	0.09	0.06 (65%)	0.06 (72%)	0.07 (83%)
(B) At Cu K-edge (9016 eV)				
$[Zn_{1.5}Cu_{1.5}Ga(OH)_8]_2^+(CO_3)^{2-}\cdot mH_2O$	0.08	0.06 (76%)	0.07 (87%)	0.08 (91%)
(C) At Ga K-edge (10,397–10,398 eV)				
$[Zn_3Ga(OH)_8]_2^+(CO_3)^{2-}\cdot mH_2O$	0.23	0.16 (70%)	0.16 (70%)	0.16 (70%)
$[Zn_{1.5}Cu_{1.5}Ga(OH)_8]_2^+(CO_3)^{2-}\cdot mH_2O$	0.29	0.22 (76%)	0.22 (76%)	0.24 (84%)

[a] Values in parentheses: peak intensity ratio to the as-synthesized sample.

$[Zn_{1.5}Cu_{1.5}Ga(OH)_8]_2^+(CO_3)^{2-}\cdot mH_2O$ were not observed for the first postedge peak at 9688 eV for $[ZnGa(OH)_8]_2^+(CO_3)^{2-}\cdot mH_2O$ (Fig. 5D). The peak intensity decreased to 64% of that for the fresh one in vacuum at 383 K and remained unchanged in CO_2 at 290–423 K (Table 2), suggesting specific interaction of Cu sites with CO_2 molecules.

The intensity of the first postedge peak of the Ga K-edge XANES of the fresh $[Zn_{1.5}Cu_{1.5}Ga(OH)_8]_2^+(CO_3)^{2-}\cdot mH_2O$ sample at 10,398 eV decreased to 76% by heating at 383 K (Fig. 5C-e → e-383). The peak intensity remained the same upon introducing CO_2 at 290 K (spectrum e-CO_2-290), but it increased again to 84% of that of the fresh sample at 423 K (spectrum e-CO_2-423, Table 2C). In $[Zn_{1.5}Cu_{1.5}Ga(OH)_8]_2^+(CO_3)^{2-}\cdot mH_2O$, the extent of recovery of the first postedge peak intensity due to the interaction with CO_2 was in the following order: Cu sites > Zn sites > Ga sites. The peak recovery was always enhanced by heating from 290 to 423 K, suggesting activated sorption of CO_2 between the LDH layers.

Table 3
Photocatalytic rates of CO_2 reduction with H_2 using LDH and reference photocatalysts.[a]

I

Photocatalyst	Formation rate (nmol h^{-1} g_{cat}^{-1})			Quantum yield (ppm)[f]			Conversion	Selectivity to CH_3OH (mol%)
	CH_3OH	CO	Σ	CH_3OH	CO	Σ	(%, C-base)	
(A) In H_2 (21.7 kPa)								
$[Zn_3Ga(OH)_8]_2^+(CO_3)^{2-}\cdot mH_2O$	13 (±1)	30 (±2)	43				0.01[b]	30 (±3)
$[Zn_{1.5}Cu_{1.5}Ga(OH)_8]_2^+(CO_3)^{2-}\cdot mH_2O$	42 (±3)	66 (±5)	110				0.02[b]	39 (±4)
(B) In CO_2 (2.3 kPa) + H_2 (21.7 kPa)								
$[Zn_3Ga(OH)_8]_2^+(CO_3)^{2-}\cdot mH_2O$	51 (±4)	80 (±6)	130	2.8	0.83	3.6	0.02	39 (±4)
$[Zn_{1.5}Cu_{1.5}Ga(OH)_8]_2^+(CO_3)^{2-}\cdot mH_2O$	170 (±14)	79 (±6	250	1.5	0.19	1.7	0.03	68 (±4)
$[Zn_3Al(OH)_8]_2^+(CO_3)^{2-}\cdot mH_2O$	39 (±3)	620 (±6)	660				0.16	5.9 (±0.5)
$[Zn_{1.5}Cu_{1.5}Al(OH)_8]_2^+(CO_3)^{2-}\cdot mH_2O$	130 (±10)	370 (±4)	500				0.11	26 (±2)
$[Zn_{1.5}Cu_{1.5}Al(OH)_8]_2^+(CO_3)^{2-}\cdot mH_2O$[c]	200 (±16)	580 (±6)	780				0.16	26 (±2)
Cu—ZnO[d]	<2	30 (±2)	30				0.006	<7
Ga_2O_3[e]	<2	47 (±3)	47				0.01	<4

II

Photocatalyst	Formation rate per specific surface area (nmol h^{-1} m^{-2})			Formation rate per amount of Cu (nmol h^{-1} $mmol_{Cu}^{-1}$)		
	CH_3OH	CO	Σ	CH_3OH	CO	Σ
(A) In H_2 (21.7 kPa)						
$[Zn_3Ga(OH)_8]_2^+(CO_3)^{2-}\cdot mH_2O$	0.19	0.43	0.62	–	–	–
$[Zn_{1.5}Cu_{1.5}Ga(OH)_8]_2^+(CO_3)^{2-}\cdot mH_2O$	0.74	1.2	1.9	13	20	34
(B) In CO_2 (2.3 kPa) + H_2 (21.7 kPa)						
$[Zn_3Ga(OH)_8]_2^+(CO_3)^{2-}\cdot mH_2O$	0.73	1.1	1.9	–	–	–
$[Zn_{1.5}Cu_{1.5}Ga(OH)_8]_2^+(CO_3)^{2-}\cdot mH_2O$	3.0	1.4	4.4	53	25	78
$[Zn_3Al(OH)_8]_2^+(CO_3)^{2-}\cdot mH_2O$	0.68	11	12	–	–	–
$[Zn_{1.5}Cu_{1.5}Al(OH)_8]_2^+(CO_3)^{2-}\cdot mH_2O$	3.4	9.7	13	37	100	140
$[Zn_{1.5}Cu_{1.5}Al(OH)_8]_2^+(CO_3)^{2-}\cdot mH_2O$[c]	5.3	15	21	56	160	220
Cu—ZnO[d]	<0.05	0.73	0.73	<0.30	4.5	4.5
Ga_2O_3[e]	<1	23	23	–	–	–

[a] The catalyst amount was 100 mg. Values in parentheses are experimental errors for evaluation.
[b] Calculated on the basis of molar amount of interlayer carbonate ions converted to methanol and CO.
[c] The photon flux illuminated using Model SX-UID502XAM was 2.5 times greater than other photocatalytic tests using Model UI-502Q in the comparison of the whole wavelength region.
[d] The Cu—ZnO catalyst was prepared via the reported inverse precipitation method starting from copper and zinc nitrates (atomic ratio Cu:Zn = 54:46) with $NaHCO_3$ [27].
[e] Commercial sample (Kanto Chemical, 99.0%). The major crystalline phase was α-Ga_2O_3.
[f] Transmitted light intensity (Fig. S3) was subtracted from the incident light intensity for the evaluation.

Similarly to the first postedge in the Zn K-edge for $[Zn_3Ga(OH)_8]_2^+(CO_3)^{2-} \cdot mH_2O$, the intensity of the first postedge peak in the Ga K-edge spectrum decreased to 70% of the fresh one and remained the same in CO_2 at 290–423 K (Fig. 5E and Table 2C, A), suggesting poor interaction of the Zn/Ga sites with CO_2 molecules.

3.4. Photocatalytic reduction rates of CO_2

First, the reactivity of the interlayer carbonate ions of LDHs was tested in 21.7 kPa of H_2 for $[Zn_{3-x}Cu_xGa(OH)_8]_2^+(CO_3)^{2-} \cdot mH_2O$ (x = 0, 1.5) (Table 3I-A and Fig. 6A and B). Methanol was detected as a byproduct using both catalysts under UV–visible light in addition to the major product of CO (70–61 mol%). The conversion of carbonate ions into methanol + CO was 0.01–0.02%.

The photocatalysis of $[Zn_3Ga(OH)_8]_2^+(CO_3)^{2-} \cdot mH_2O$ was tested in 2.3 kPa of CO_2 + 21.7 kPa of H_2 under illumination by UV–visible light (Fig. 6C). The major product was CO (selectivity 61 mol%), and methanol was also formed. The catalyst was compared to $[Zn_{1.5}Cu_{1.5}Ga(OH)_8]_2^+(CO_3)^{2-} \cdot mH_2O$ (Fig. 6D). The formation rate of CO was essentially identical (79 nmol $h^{-1}g_{cat}^{-1}$), whereas that of methanol increased (170 nmol $h^{-1}g_{cat}^{-1}$) by a factor of 3.3 for $[Zn_{1.5}Cu_{1.5}Ga(OH)_8]_2(CO_3)^{2-} \cdot mH_2O$. The methanol selectivity was improved to 68 mol% (Table 3I-B).

Next, the $[Zn_3Al(OH)_8]_2^+(CO_3)^{2-} \cdot mH_2O$ catalyst was tested (Fig. 6E) in comparison to the $[Zn_3Ga(OH)_8]_2^+(CO_3)^{2-} \cdot mH_2O$ catalyst (Fig. 6C). Total product formation rate was enhanced by a factor of 5.1 of $[Zn_3Ga(OH)_8]_2^+(CO_3)^{2-} \cdot mH_2O$ by the substitution of Ga for Al. The major product was CO (selectivity 94 mol%). Then the $[Zn_{1.5}Cu_{1.5}Al(OH)_8]_2^+(CO_3)^{2-} \cdot mH_2O$ catalyst (Fig. 6F) was compared to the $[Zn_3Al(OH)_8]_2^+(CO_3)^{2-} \cdot mH_2O$ catalyst. The total product formation rate decreased by 24%. Similarly to the Cu substitution into $[Zn_3Ga(OH)_8]_2^+(CO_3)^{2-} \cdot mH_2O$, the methanol formation rate was promoted by a factor of 3.3 of $[Zn_3Al(OH)_8]_2^+(CO_3)^{2-} \cdot mH_2O$. The conversion using $[Zn_{1.5}Cu_{1.5}Al(OH)_8]_2^+(CO_3)^{2-} \cdot mH_2O$ was improved by increasing the light intensity of Model UI-502Q (0.11%) to 2.5 times using Model SX-UID502XAM (0.16%, Table 3I-B) in the comparison of the whole wavelength region.

The formation rates per specific surface area of catalyst and those per amount of Cu are also summarized in Table 3II. Especially, a concern that 500-W high-intensity light may lead to a local high temperature for the catalyst can be estimated based on the formation rates per amount of Cu, although the catalyst temperature was monitored to be 305–313 K (Fig. S2). Conventional Cu—ZnO catalyst was quite inactive per amount of Cu and formed only CO. The Cu sites in LDH are Cu^{II}, which is normally considered to be inactive for thermal methanol synthesis [27]. Further, LDHs that do not contain Cu ($[Zn_3Ga(OH)_8]_2^+(CO_3)^{2-} \cdot mH_2O$, $[Zn_3Al(OH)_8]_2^+(CO_3)^{2-} \cdot mH_2O$) did produce methanol (Table 3I-B). Thus, the catalysis listed in Table 3 should be photocatalytic below 313 K.

The formation rates of water were between 0.5 and 2.0 μmol $h^{-1}g_{cat}^{-1}$ in the kinetic tests (Fig. 6C–F). These rates exceed the amount of water that was catalytically formed as the products of the following equations:

$$CO_2 + H_2 \rightarrow CO + H_2O$$

$$CO_2 + 3H_2 \rightarrow CH_3OH + H_2O.$$

This discrepancy is due to the desorption of interlayer water molecules of LDHs [15–19].

A control reaction experiment was performed using $[Zn_{1.5}Cu_{1.5}Al(OH)_8]_2^+(CO_3)^{2-} \cdot mH_2O$ in the absence of light (Fig. 6BL-2). Another control experiment included a reaction

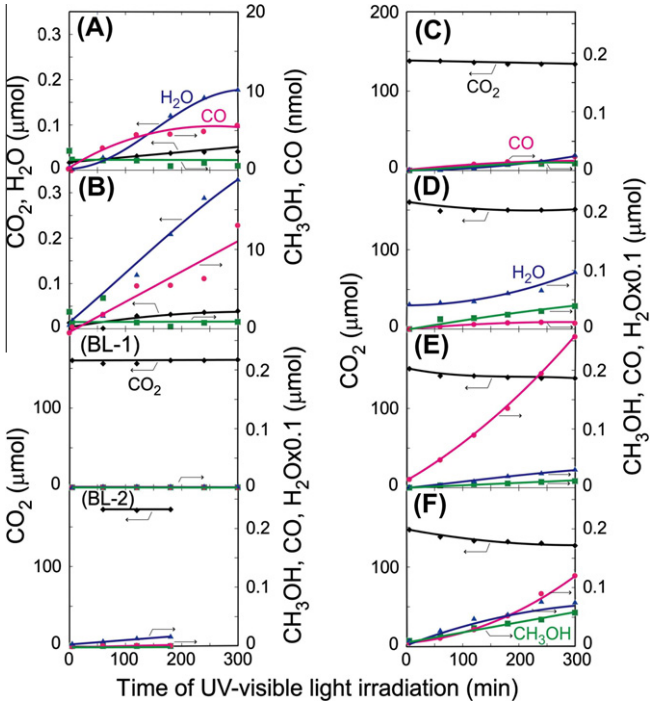

Fig. 6. Time course of photoreactions in only H_2 alone (21.7 kPa; A, B) and in CO_2 (2.3 kPa) + H_2 (21.7 kPa) (C–F, BL-1, BL-2). One hundred milligrams of the LDH catalyst was charged except for the blank test BL-1 (empty reactor): $[Zn_3Ga(OH)_8]_2^+(CO_3)^{2-} \cdot mH_2O$ (A, C), $[Zn_{1.5}Cu_{1.5}Ga(OH)_8]_2^+(CO_3)^{2-} \cdot mH_2O$ (B, D), $[Zn_3Al(OH)_8]_2^+(CO_3)^{2-} \cdot mH_2O$ (E), and $[Zn_{1.5}Cu_{1.5}Al(OH)_8]_2^+(CO_3)^{2-} \cdot mH_2O$ (F, BL-2). The reactor was illuminated with a 500-W Xe arc lamp except for blank test BL-2 (reactor in darkness). CO_2 (♦; diamond), H_2O (▲; triangle), CH_3OH (■; square), and CO (●; circle).

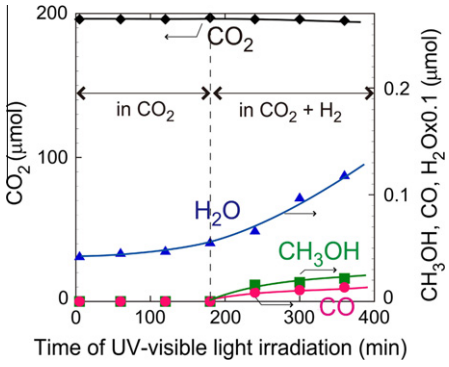

Fig. 7. Time course of photoreactions in CO_2 (2.6 kPa) only in first 3 h and in CO_2 (2.6 kPa) + H_2 (21.7 kPa) after 3 h from the start of the reactions for 100 mg of $[Zn_{1.5}Cu_{1.5}Ga(OH)_8]_2^+(CO_3)^{2-} \cdot mH_2O$. Other reaction conditions and legends are the same as those for Fig. 6.

Table 4
Comparison of photoconversion of gases over $[Zn_{1.5}Cu_{1.5}Ga(OH)_8]_2^+(CO_3)^{2-} \cdot mH_2O$[a].

Condition	Formation rate (nmol h^{-1} g_{cat}^{-1})	
	CH_3OH	CO
In methanol (1.7 Pa), no light	–	<2
In methanol (1.7 Pa), under light[b]	−26	26
In methanol (1.7 Pa) + H_2 (21.7 kPa), no light	–	<2
In methanol (1.7 Pa) + H_2 (21.7 kPa), under light[b]	24	82
In H_2 (21.7 kPa), under light[b]	42	66

[a] The catalyst amount was 100 mg.
[b] Photocatalytic tests using Model UI-502Q.

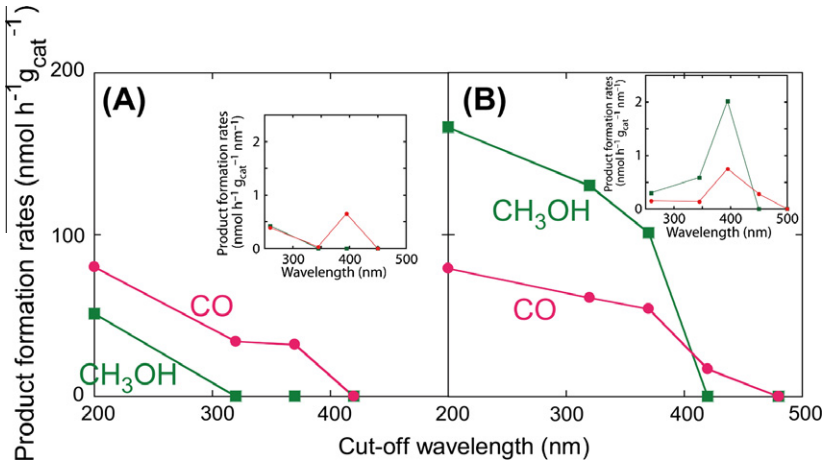

Fig. 8. Dependence of the formation rates of methanol and CO on the cutoff wavelength for the photoreactions in CO_2 (2.3 kPa) + H_2 (21.7 kPa) for 100 mg of $[Zn_3Ga(OH)_8]_2^+(CO_3)^{2-} \cdot mH_2O$ (A) or $[Zn_{1.5}Cu_{1.5}Ga(OH)_8]_2^+(CO_3)^{2-} \cdot mH_2O$ (B). Sharp cutoff filters UV-32, L-37, L-42, or Y-48 were used at the exit of the Xe arc lamp. Other reaction conditions and legends are the same as those for Fig. 6. (Inset) Action spectrum of product formation rates vs wavelength.

without any catalyst under the illumination of UV–visible light (reactor only, Fig. 6BL-1). In both experiments, methanol and CO were not found.

To ensure methanol formation starting from gaseous CO_2 and H_2, the products were monitored when $[Zn_{1.5}Cu_{1.5}Ga(OH)_8]_2^+(CO_3)^{2-} \cdot mH_2O$ was in 2.6 kPa of CO_2 for the first 3 h under UV–visible light and then 21.7 kPa of H_2 was added for the next 3 h, keeping the UV–visible light on (Fig. 7). Methanol was not observed during the first 3 h; however, upon the addition of H_2 gas, methanol formation started at a rate of 160 nmol $h^{-1}g_{cat}^{-1}$ over the next 3 h. The formation rate was similar to that observed in Fig. 6D. The methanol formation rate was only 42 nmol $h^{-1}g_{cat}^{-1}$ for the reaction of interlayer carbonate with gaseous H_2 (Table 3A). Thus, methanol was formed predominantly starting from gaseous $CO_2 + H_2$ using $[Zn_{1.5}Cu_{1.5}Ga(OH)_8]_2^+(CO_3)^{2-} \cdot mH_2O$.

The stability of 1.7 Pa (0.13 μmol) of methanol was checked over $[Zn_{1.5}Cu_{1.5}Ga(OH)_8]_2^+(CO_3)^{2-} \cdot mH_2O$ in the presence/absence of light and with/without H_2. Methanol was stable in the absence of light both with and without H_2, and no CO desorption was observed (Table 4). Instead, methanol adsorbed on $[Zn_{1.5}Cu_{1.5}Ga(OH)_8]_2^+(CO_3)^{2-} \cdot mH_2O$ at a rate of (more than) 510 nmol $h^{-1}g_{cat}^{-1}$ within 1 h.

Next, when the catalyst was under UV–visible light without H_2, most of adsorbed methanol desorbed within 15 min. The formation rate of CO was 26 nmol h^{-1} g_{cat}^{-1}, starting from methanol. When the catalyst was under UV–visible light with H_2, most of the adsorbed methanol desorbed within 15 min again. The formation rate of CO was 82 nmol h^{-1} g_{cat}^{-1} starting from both methanol and the interlayer carbonate of LDH. The methanol amount increased at 24 nmol h^{-1} g_{cat}^{-1} due to the balance of formation starting from carbonate of LDH reacted with H_2 (42 nmol h^{-1} g_{cat}^{-1} under a similar photoreaction condition, Table 3A) and photodecomposition to CO (Table 4).

3.5. Dependence of photocatalytic reduction of CO_2 on light wavelength and catalyst durability

The dependence of rates of methanol and CO formation from $CO_2 + H_2$ gases on light wavelength was investigated for $[Zn_3Ga(OH)_8]_2^+(CO_3)^{2-} \cdot mH_2O$ and $[Zn_{1.5}Cu_{1.5}Ga(OH)_8]_2^+(CO_3)^{2-} \cdot mH_2O$ photocatalysts using several sharp cutoff filters (Fig. 8).

Methanol formation using $[Zn_3Ga(OH)_8]_2^+(CO_3)^{2-} \cdot mH_2O$ decreased sharply as the cutoff wavelength increased to 320 nm (Fig. 8A) in accordance with the UV absorption edge, which can be extrapolated to 222 nm (Fig. 3A-c). In addition, the CO formation rate dropped as the cutoff wavelength increased; however, a significant rate of formation (32 nmol h^{-1} g_{cat}^{-1}) was observed when the cutoff wavelength was 370 nm. This trend may originate from the UV absorption peak between 260 and 375 nm at the foot of the main absorption edge for $[Zn_3Ga(OH)_8]_2^+(CO_3)^{2-} \cdot mH_2O$ (Fig. 3A, inset c). The additional UV light absorption could be related to the surface sites of LDH to transform CO_2 to CO. When the cutoff wavelength was 420 nm, products were not detected using $[Zn_3Ga(OH)_8]_2^+(CO_3)^{2-} \cdot mH_2O$.

$[Zn_{1.5}Cu_{1.5}Ga(OH)_8]_2^+(CO_3)^{2-} \cdot mH_2O$ was photocatalytically active when the cutoff wavelength was less than 370 nm, but the activity decreased to zero when the cutoff wavelength was 420 nm (methanol formation) or 480 nm (CO formation) (Fig. 8B). This dependence is principally in accord with the UV–visible absorption edge, which can be extrapolated to 354 nm, but slower CO formation when the cutoff wavelength was 420 nm could be ascribed to a shoulder peak at the foot of the UV absorption edge and/or small visible light absorption between 400 and 480 nm (Fig. 3A-d). These trends are also clear in the action spectra as insets of Fig. 8A and B. Major product formation corresponded to wavelengths less than 320 nm for $[Zn_3Ga(OH)_8]_2^+(CO_3)^{2-} \cdot mH_2O$, whereas both methanol and CO formation corresponded to wavelengths centered at 390 nm for $[Zn_{1.5}Cu_{1.5}Ga(OH)_8]_2^+(CO_3)^{2-} \cdot mH_2O$.

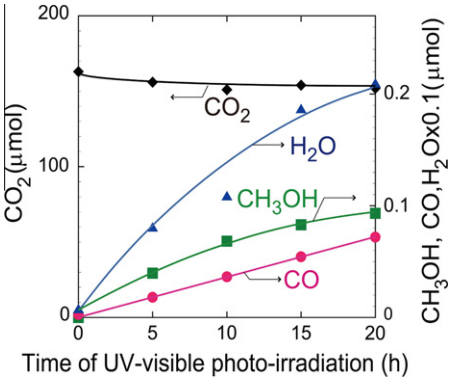

Fig. 9. Time course of photoreactions in CO_2 (2.3 kPa) + H_2 (21.7 kPa) for 100 mg of $[Zn_{1.5}Cu_{1.5}Ga(OH)_8]_2^+(CO_3)^{2-} \cdot mH_2O$ for 20 h. Other reaction conditions and legends are the same as those for Fig. 6.

Finally, the durability of the $[Zn_{1.5}Cu_{1.5}Ga(OH)_8]_2^+(CO_3)^{2-} \cdot mH_2O$ catalyst was tested for 20 h. The photocatalyst exhibited the best selectivity to methanol (68 mol%) in 5 h (Table 3B and Fig. 6D). In the 20-h test, methanol formation continued and the selectivity was 68–57 mol% (Fig. 9). In every 5 h, the methanol formation rate gradually decreased, starting from 79, to 57, 30, and then 19 nmol h^{-1} g_{cat}^{-1}, whereas the CO formation rate remained constant (36 nmol h^{-1} g_{cat}^{-1}) for 20 h. Throughout the 20-h test, no other products were found except for methanol, CO, and water.

4. Discussion

4.1. Catalyst syntheses and photocatalysis

LDH compounds were synthesized with chemical compositions $[Zn_{3-x}Cu_xM^{III}(OH)_8]_2^+(CO_3)^{2-} \cdot mH_2O$, where M was Al or Ga and the x value was 0–1.5. The synthesis of the LDH structure was confirmed on the basis of the XRD spectra (Fig. 1a–c). The divalent Cu was successfully incorporated into the octahedral sites in the cationic layers with a maximum Cu:Zn atomic ratio of 1:1, as confirmed by Cu and Zn K-edge XANES spectra (Fig. 4A and B). The incorporation of Cu with a maximum Cu:Zn atomic ratio of 7:3 was reported for $[Zn_{3-x}Cu_xAl^{III}(OH)_8]_2^+(CO_3)^{2-} \cdot mH_2O$ [27]. In the case where M was Ga and the x value was 1.5, the diffraction peaks derived from the impurity phase(s) were observed in the XRD spectrum at $2\theta_B = 27.9°$, 30.3°, 35.7°, 57.3°, and 62.9° (Fig. 1d). The S_{BET} value of $[Zn_3Ga^{III}(OH)_8]_2^+(CO_3)^{2-} \cdot mH_2O$ was slightly higher (70 m^2 g^{-1}) than that of $[Zn_3Al^{III}(OH)_8]_2^+(CO_3)^{2-} \cdot mH_2O$ (57 m^2 g^{-1}; Table 1). The S_{BET} value decreased by 19–34% when equimolar amounts of Cu and Zn metal were included in the LDHs and when M was either Al or Ga. The coagulated flat flakes smaller than 100 nm in the SEM images were suggested to be stacked layers of $[Zn_3Al(OH)_8]_2^+(CO_3)^{2-} \cdot mH_2O$ (Fig. 2).

Synthesized LDHs formulated as $[Zn_{3-x}Cu_xM^{III}(OH)_8]_2^+(CO_3)^{2-} \cdot mH_2O$ were applied to the photocatalytic reduction of CO_2 (Table 3 and Fig. 6). First, the conversion of interlayer carbonate ions of $[Zn_{3-x}Cu_xGa(OH)_8]_2^+(CO_3)^{2-} \cdot mH_2O$ ($x = 0, 1.5$) was tested in the presence of H_2 gas. Methanol formation was confirmed at rates of 13—42 nmol $h^{-1}g_{cat}^{-1}$ and the total conversion of carbonate to methanol + CO was 0.01–0.02% (Table 3A). The CO_2 formation derived from the carbonate ions was of the same or a slightly higher order than the formation of methanol and CO (Fig. 6A and B). Because the interlayer carbonate ions balance the charge with the $[Zn_{3-x}Cu_xGa(OH)_8]^+$ cation layers, it could be difficult to convert and remove carbonate ions from the interlayer space if an extra carbonate source or alternative anion source were not provided.

Photocatalytic methanol formation tests were performed in the presence of CO_2 and H_2 gases using several LDH samples in comparison to a conventional Cu—ZnO catalyst and Ga_2O_3, which have primarily an α-crystalline phase (Table 3B). This is the first report to synthesize methanol starting from CO_2 and H_2 using photocatalysts under only UV–visible light. When $[Zn_{3-x}Cu_xAl(OH)_8]_2^+(CO_3)^{2-} \cdot mH_2O$ ($x = 0, 1.5$) catalysts were used, CO (selectivity 94–74 mol%) was a major product. In this study, exclusive CO photoformation was reported using Rh/TiO_2 [29], ZrO_2 [30,31], MgO [32], and Ga_2O_3 [33], and was observed using Cu—ZnO or Ga_2O_3 (Table 3B). Among the LDH samples tested in this study, $[Zn_{3-x}Cu_xAl(OH)_8]_2^+(CO_3)^{2-} \cdot mH_2O$ catalysts were the most active. The conversions (0.16–0.11%) were an order of magnitude greater than those obtained using references Cu—ZnO and Ga_2O_3 (0.01–0.006%). The formation of methanol + CO was accelerated by increasing the light intensity (500 nmol h^{-1} g_{cat}^{-1}) to 2.5 times (780 nmol h^{-1} g_{cat}^{-1}) for $[Zn_{1.5}Cu_{1.5}Al(OH)_8]_2(CO_3)^{2-} \cdot mH_2O$ in the comparison of the whole wavelength region. Methanol was the major product when the $[Zn_{1.5}Cu_{1.5}Ga(OH)_8]_2(CO_3)^{2-} \cdot mH_2O$ photocatalyst was used (selectivity 68 mol%; Table 3I-B). Photocatalytic conversion of CO_2 into methanol in aqueous solution was reported using Co-phthalocyanine/TiO_2 [11] and Nd^{3+}/TiO_2 [12]. The maximum formation rates of methanol were 9.3 and 23 μmol h^{-1} g_{cat}^{-1}, respectively, in addition to a higher formation rate of formic acid using CoPc/TiO_2 (150 μmol h^{-1} g_{cat}^{-1}). The disadvantage of LDH catalysts for slower photoconversion of CO_2 using hydrogen in this study may be due to slow gas diffusion in the interlayer space compared to the cases in these references.

The dependence of the photocatalytic methanol formation rate on the light wavelength (Fig. 8) was compared to the UV–visible absorption spectra for $[Zn_3Ga(OH)_8]_2(CO_3)^{2-} \cdot mH_2O$ (Fig. 3A-c and A-d). The higher limit of the wavelength used to form methanol was between 370 and 420 nm for $[Zn_{1.5}Cu_{1.5}Ga(OH)_8]_2^+(CO_3)^{2-} \cdot mH_2O$ (Fig. 8B), in accordance with the UV absorption edge extrapolated to 354 nm or the foot (400 nm) of a smaller shoulder on the absorption edge (Fig. 3A-d). The higher limit of wavelengths at which methanol formed was less than 320 nm for $[Zn_3Ga(OH)_8]_2^+(CO_3)^{2-} \cdot mH_2O$ (Fig. 8A), in accordance with the UV absorption edge extrapolated to 222 nm (Fig. 3A-c). The CO formation rates also decreased as the cutoff wavelength increased; however, the trend was less steep than for methanol, and thus, the CO selectivity was 100 mol% when the cutoff wavelength was 370 nm ($[Zn_3Ga(OH)_8]_2^+(CO_3)^{2-} \cdot mH_2O$) and 420 nm ($[Zn_{1.5}Cu_{1.5}Ga(OH)_8]_2^+(CO_3)^{2-} \cdot mH_2O$) (Fig. 8). These minor differences probably occur because the UV–visible absorption is the electronic transition to the energy level slightly below the bottom of the conduction band and this level was derived from the surface sites selective for transforming CO_2 into CO.

The action spectra in the insets of Fig. 8A and B were compared to the light intensity distribution for Model UI-502Q obtained using a USR40 spectroradiometer (Ushio). Compared to the light intensity peak centered at 380 nm (not shown), the quantum yield for methanol formation using $[Zn_{1.5}Cu_{1.5}Ga(OH)_8]_2^+(CO_3)^{2-} \cdot mH_2O$ was evaluated at 1.5 ppm (Table 3I-B). The quantum yield for all products was 1.7 ppm. On the other hand, the action spectrum for $[Zn_3Ga(OH)_8]_2^+(CO_3)^{2-} \cdot mH_2O$ (Fig. 8A, inset) was compared to the light intensity peak centered at 315 nm. The quantum yields for methanol and CO were 2.8 and 0.83 ppm, respectively (Table 3I-B). As the bandgap of LDHs that do not contain Cu was wider (5.6–5.7 eV), they would utilize UV light only between 200 and 220 nm (Fig. 3A).

The methanol formation and minor CO formation using the $[Zn_{1.5}Cu_{1.5}Ga(OH)_8]_2^+(CO_3)^{2-} \cdot mH_2O$ photocatalyst was confirmed for as long as 20 h (Fig. 9), suggesting the suitability of the photocatalysts to capturing CO_2 and converting it to fuel under continuous natural light. The gradual decrease of the methanol formation rate may be affected by the readsorption of product methanol in contrast to the constant formation rate for CO, because product CO readsorption on $[Zn_{1.5}Cu_{1.5}Ga(OH)_8]_2^+(CO_3)^{2-} \cdot mH_2O$ catalyst should be weaker.

For $[Zn_{1.5}Cu_{1.5}Ga(OH)_8]_2^+(CO_3)^{2-} \cdot mH_2O$ under UV–visible light, the methanol formation rates increased from 42 nmol h^{-1} g_{cat}^{-1} in H_2 to 170 nmol h^{-1} g_{cat}^{-1} in $CO_2 + H_2$ (Table 3). The presence of carbonate is possibly the key to methanol photosynthesis; however, gaseous CO_2 promoted the formation rates by a factor of 4.0. On the other hand, the catalyst under UV–visible light produced no product in CO_2 and the photocatalysis required the addition of H_2 to the system (Fig. 7). No methanol was detected after the catalyst was suspended in deionized water under UV–visible light for 5 h (see the Supporting materials). Furthermore, no impurity that contained carbon was included in the reagents used throughout the LDH syntheses, except for sodium carbonate. Therefore, the source of methanol was gaseous CO_2 and interlayer carbonates. The photoconversion of carbonates to methanol was favorable in

the presence of gaseous CO_2 and it most likely compensated for the interlayer anions.

4.2. Spectroscopic insight and reaction mechanism of photocatalysis

The specific photocatalysis thus found to form methanol from CO_2 were correlated with the desorption trend of interlayer molecules (water and/or carbonates) and the adsorption of the substrate. The LDH structure is ultimately simple from the viewpoint of heterogeneous catalysis because all the surface sites are hydroxy groups bound to $[MO_6]$ octahedra and the type of metal elements (Zn, Cu, Ga, or Al) is the only difference (Scheme 1A). The presence or absence of interlayer molecules was difficult to monitor using EXAFS. However, the first postedge peak (9688–9689 eV at the Zn K-edge, 9016 eV at the Cu K-edge, and 10,397–10,398 eV at the Ga K-edge) was found to be a critical indicator of the presence or absence of these molecules (Fig. 5).

For the LDH compound $[Zn_{1.5}Cu_{1.5}Ga(OH)_8]_2^+(CO_3)^{2-}\cdot mH_2O$, which was the most methanol-selective, the intensity of the first postedge peak at the Zn K-edge decreased to 65% of that for the fresh one in vacuum at 383 K due to the loss of structural water molecules and/or carbonates. The Zn K postedge peak intensity decreased similarly for Cu-free $[Zn_3Ga(OH)_8]_2^+(CO_3)^{2-}\cdot mH_2O$ to 64% of that for the fresh one. The peak intensity increased to 83% in CO_2 at 423 K in the former Cu-containing LDH, whereas the peak remained unchanged for the latter Cu-free LDH in CO_2 at 290–423 K.

The desorption–adsorption trend monitored at the Zn K-edge for $[Zn_{1.5}Cu_{1.5}Ga(OH)_8]_2^+(CO_3)^{2-}\cdot mH_2O$ was also evident in both the Cu and the Ga K-edge spectra. The recovery extent (=peak increase due to CO_2 sorption/peak decrease caused by the loss of water and carbonates) of the first postedge peak intensity in the normalized XANES spectra was of the following order: Cu sites (63%) > Zn sites (51%) > Ga sites (11%). In contrast, the first Ga K postedge peak remained unchanged for Cu-free $[Zn_3Ga(OH)_8]_2^+(CO_3)^{2-}\cdot mH_2O$ in CO_2 gas at 290–423 K.

More importantly, the methanol formation rate was enhanced by a factor of 3.3 by adding Cu to $[Zn_3Ga(OH)_8]_2^+(CO_3)^{2-}\cdot mH_2O$ (Table 3B). The Cu site should play the photocatalytic role by binding CO_2 and coupling it with protons and photogenerated electrons, presumably utilizing a Cu^I and Cu^{II} redox couple. This binding between CO_2 and Cu in turn affects the multiple scattering region of Zn and Ga sites as well, because interlayer hydroxy groups shared by Cu and Zn (Scheme 2a, M = Zn) and by Cu and Ga (Scheme 2a, M = Ga) inserted CO_2 to form hydrogen carbonate (Schemes 2b and 1B). The steps b → c → d in Scheme 2 should be promoted utilizing the Cu^I and Cu^{II} redox couple. Further reduction steps e → f, f → g, g → h, and h → a should be also coupled with the Cu^I and Cu^{II} redox to finally produce methanol. If the species e is dehydrated, another catalytic cycle can be proposed to regenerate species a. A clear explanation cannot be given at the moment for why methanol and CO were exclusively obtained in the catalytic cycles of Scheme 2. Formic acid and formaldehyde may be unstable and/or insensitive by the gas-phase sampling of heterogeneous catalysis using GC.

The role of the Cu^I sites supported on TiO_2 in the CO_2 photoreduction in alkaline aqueous solution under the UV light was suggested [48]. The formation of carbonate species over a MgO catalyst was proposed, but the previous studies suggested it to be inactive or to only lead to CO formation in H_2 gas [32]. The discrepancy between these previous studies and this study should be due to the presence or absence of Cu sites.

Photocatalytic activity of $[Zn_{3-x}Cu_xAl(OH)_8]_2^+(CO_3)^{2-}\cdot mH_2O$ was greater than that of $[Zn_{3-x}Cu_xGa(OH)_8]_2^+(CO_3)^{2-}\cdot mH_2O$. The exact photocatalytic role of M^{III} sites is not known at present. One of the possibilities is the 50-nm difference of the UV light absorption edge between M^{III} = Ga and Al (Fig. 3A-d and A-b). The peaks of product formation rates in the action spectrum for $[Zn_{1.5}Cu_{1.5}Ga(OH)_8]_2^+(CO_3)^{2-}\cdot mH_2O$ centered at 390 nm (Fig. 8B, inset) were fairly close to the light intensity peak from the Xe arc lamp centered at 380 nm. The wavelength shift of 50 nm toward the higher energy side for $[Zn_{1.5}Cu_{1.5}Al(OH)_8]_2^+(CO_3)^{2-}\cdot mH_2O$ may be serious because intense light centered at 380 nm did not contribute to the charge separation for the catalyst. A decrease in basicity from substituting an Al site for Ga in the layered structure was reported [49]. The affinity of Ga sites in LDHs with CO_2 was suggested [26].

The photocatalytic energetic is depicted in Scheme 3. The bandgap values (5.7–4.1 eV) estimated for $[Zn_3Al(OH)_8]_2^+(CO_3)^{2-}\cdot mH_2^+O$ and $[Zn_{1.5}Cu_{1.5}Al(OH)_8]_2(CO_3)^{2-}\cdot mH_2O$ were greater than that for ZnO, enabling CO_2 photoreduction at relatively higher potentials to form methanol at −0.32 V and to form CO at −0.11 V by supplying photoexcited electrons to CO_2 in the conduction band. On the other hand, photogenerated holes in the valence band were neutralized with electrons formed during H_2 oxidation (0 V). This trend and electron flow are also evident for $[Zn_{3-x}Cu_xGa(OH)_8]_2^+(CO_3)^{2-}\cdot mH_2O$ (bandgap values estimated as 5.6–3.5 eV; Table 1B). The selectivity to produce methanol vs CO formation increased by adding Cu to $[Zn_3M^{III}(OH)_8]_2^+(CO_3)^{2-}\cdot mH_2O$ (M = Al, Ga; Table 3). The bandgap became narrower with the addition of Cu; however, the potential for the methanol formation step ($CO_2 + 6H^+ + 6e^- \rightarrow CH_3OH + H_2O$) [2] was 0.21 V higher than that for the CO formation step (Scheme 3).

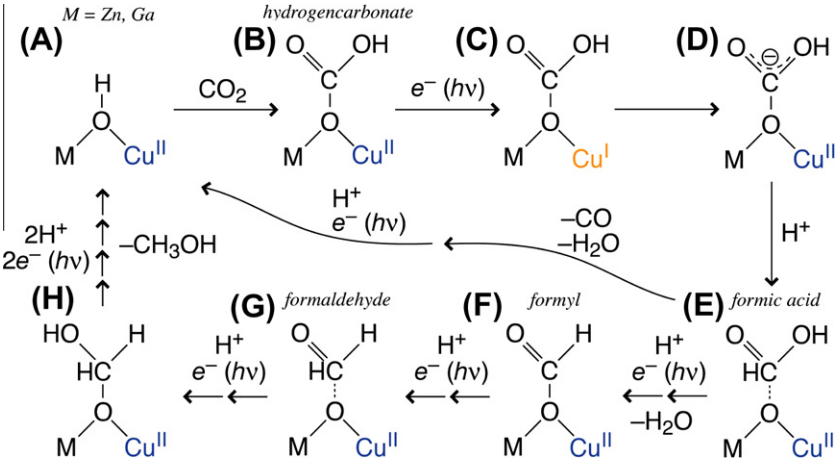

Scheme 2. Proposed photocatalytic catalytic cycle of CO_2 reduction to methanol or CO over Zn—Cu—Ga LDH catalysts.

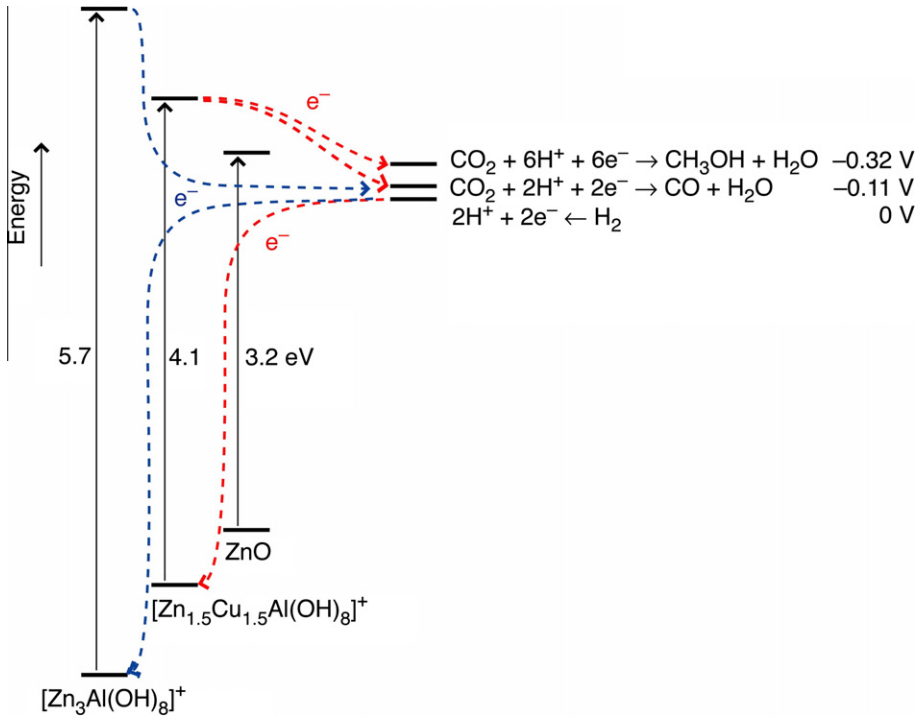

Scheme 3. Energy levels at the bandgap for ZnO, $[Zn_{1.5}Cu_{1.5}Al(OH)_8]_2^+(CO_3)^{2-}\cdot mH_2O$, and $[Zn_3Al(OH)_8]_2^+(CO_3)^{2-}\cdot mH_2O$ vs the reaction potentials for each step of CO_2 reduction to methanol/CO and H_2 oxidation to protons.

Thus, the selectivity of CO_2 photoreduction was not controlled by the energetics of reaction steps in the viewpoint of electron flow [36,45,50–52], but the adsorption of CO_2 and the stability of the reduced species, as probed by Zn, Cu, and Ga K-edge XANES spectra (Fig. 5), should be critical.

5. Conclusions

LDH compounds formulated as $[Zn_{3-x}Cu_xM^{III}(OH)_8]_2^+(CO_3)^{2-}\cdot mH_2^+O$, where x was within the range 0–1.5 and M was Al^{III} or Ga^{III}, were synthesized and an ordered layer structure consisting of octahedral Zn, Cu, Al, and/or Ga sites was confirmed. Under UV–visible light illumination, these LDH compounds synthesized methanol starting from $CO_2 + H_2$ for the first time. $[Zn_3Al(OH)_8]_2^+(CO_3)^{2-}\cdot mH_2O$ was the most active, producing CO with 94 mol% selectivity (0.16% conversion). $[Zn_{1.5}Cu_{1.5}Ga(OH)_8]_2^+(CO_3)^{2-}\cdot mH_2O$ was the most selective for producing methanol (68 mol%) at 0.03% conversion. The photocatalytic rates can be enhanced 45% by increasing the light intensity by 2.5 times in the comparison of the whole wavelength region. Catalytic methanol formation was confirmed on the basis of blank tests performed in the absence of a catalyst under UV–visible light, in the absence of any light with a catalyst, in H_2 or CO_2 gas with a catalyst under UV–visible light, dependence on cutoff wavelength, and suspended catalyst in deionized water under UV–visible light. The inclusion of Cu sites in the LDH layers improved the methanol selectivity. The bandgap (3.5–5.7 eV) was wide enough to proceed with the reaction steps $CO_2 + 6H^+ + 6e^- \rightarrow CH_3OH + H_2O$ and $CO_2 + 2H^+ + 2e^- \rightarrow CO + H_2O$ at relatively negative reaction potentials. The key factor for determining the selectivity to methanol vs CO was suggested to be the binding of CO_2 at the Cu sites as hydrogen carbonate species Cu—O(—Zn)—C(OH)═O and Cu—O(—Ga)—C(OH)═O, as demonstrated in the X-ray absorption spectra.

Supporting text to verify photocatalytic methanol formation derived from CO_2: Fig. S1 depicts the photocatalytic reactor used in this study, Fig. S2 monitors the temperature of the reaction cell during the photocatalysis, and Fig. S3 evaluates the transmitted light intensity through catalyst layer in the reactor.

Acknowledgments

The authors are thankful for financial support from a Grant-in-Aid for Scientific Research C (2255 0117) from MEXT (2010) and from the Promotion Section of Technology Innovation, Daikin Industries (2008–2009). The authors appreciate the setup of photocatalytic measurements by M. Morikawa and Y. Yoshida. The X-ray absorption experiments were performed with the approval of the Photon Factory Proposal Review Committee (2009G552, 2007G576). The authors thank Professor Yoshitake for the Xe arc lamp and Professors Kaneko and Kanoh for the XRD apparatus.

Appendix A. Supplementary material

Supplementary data associated with this article can be found, in the online version, at doi:10.1016/j.jcat.2011.01.004.

References

[1] A. Gore, An Inconvenient Truth, The Wylie Agency, London, UK, 2006. p. 66.
[2] C. Wang, R.L. Thompson, J. Baltrus, C. Matranga, J. Phys. Chem. Lett. 1 (2010) 48.
[3] H. Takeda, K. Koike, H. Inoue, O. Ishitani, J. Am. Chem. Soc. 130 (2008) 2023.
[4] Z.H. Zhao, J.M. Fan, Z.Z. Wang, J. Cleaner Prod. 15 (2007) 1894.
[5] P. Pathak, M.J. Meziani, L. Castillo, Y.P. Sun, Green Chem. 7 (2005) 667.
[6] C.C. Yang, Y.H. Yu, B. van der Linden, J.C.S. Wu, G. Mul, J. Am. Chem. Soc. 132 (2010) 8398.
[7] I.H. Tseng, W.C. Chang, J.C.S. Wu, Appl. Catal. B 37 (2002) 37.
[8] K.R. Thampi, J. Kiwi, M. Grätzel, Nature 327 (1987) 506.
[9] T. Inoue, A. Fujishima, S. Konishi, K. Honda, Nature 277 (1979) 637.
[10] Y. Izumi, J. Arai,T. Shimizu, Japanese Patent 2009,179046.
[11] Z. Zhao, J. Fan, M. Xie, Z. Wang, J. Cleaner Prod. 17 (2009) 1025.
[12] D. Luo, C. Chen, N. Zhang, S. Hong, H. Wu, Z. Liu, Z. Phys. Chem. 223 (2009) 1465.
[13] J.K. Hurst, Science 328 (2010) 315.
[14] W.Q. Meng, F. Li, D.G. Evans, X. Duan, J. Porous Mater. 11 (2004) 97.
[15] Z. Yong, V. Mata, A.E. Rodrigues, Ind. Eng. Chem. Res. 40 (2001) 204.
[16] P.J. Sideris, U.G. Nielsen, Z. Gan, C.P. Grey, Science 321 (2008) 113.

[17] T. Hongo, T. Iemura, A. Yamazaki, J. Ceram. Soc. Jpn. 116 (2008) 192.
[18] L. Lv, P. Sun, Z. Gu, H. Du, X. Pang, X. Tao, R. Xu, L. Xu, J. Hazard. Mater. 161 (2009) 1444.
[19] J.T. Klogregge, L. Hickey, R.L. Frost, J. Solid State Chem. 177 (2004) 4047.
[20] N. Hiyoshi, K. Yogo, T. Yashima, Chem. Lett. 37 (2008) 1266.
[21] B. Wang, A.P. Cote, H. Furukawa, M.O. Keefe, O.M. Yaghi, Nature 453 (2008) 207.
[22] C. Volzone, J.O. Rinaldi, J. Ortiga, Mater. Res. 5 (2002) 475.
[23] A. Azzouz, A. Ursu, D. Nistor, T. Sajin, E. Assaad, R. Roy, Thermochim. Acta 496 (2009) 45.
[24] Z. Yong, A.E. Rodrigues, Energy Convers. Manage. 43 (2002) 1865.
[25] E.R. van Selow, P.D. Cobden, P.A. Verbraeken, J.R. Hufton, R.W. van den Brink, Ind. Eng. Chem. Res. 48 (2009) 4184.
[26] C.T. Yavuz, B.D. Shinall, A.V. Iretskii, M.G. White, T. Golden, M. Atilhan, P.C. Ford, G.D. Stucky, Chem. Mater. 21 (2009) 3473.
[27] S. Fujita, M. Usui, H. Ito, N. Takezawa, J. Catal. 157 (1995) 403.
[28] M. Behrens, I. Kasatkin, S. Kühl, G. Weinberg, Chem. Mater. 22 (2010) 386.
[29] Y. Kohno, H. Hayashi, S. Takenaka, T. Tanaka, T. Funabiki, S. Yoshida, J. Photochem. Photobiol. A 12 (1999) 117.
[30] C.C. Lo, C.H. Hung, C.S. Yuan, J.F. Wu, Solar Energy Mater. Solar Cells 91 (2007) 1765.
[31] Y. Kohno, T. Tanaka, T. Funabiki, S. Yoshida, Chem. Commun. (1997) 841.
[32] K. Teramura, T. Tanaka, H. Ishikawa, Y. Kohno, T. Funabiki, J. Phys. Chem. B 108 (2004) 346.
[33] K. Teramura, H. Tsuneoka, T. Shishido, T. Tanaka, Chem. Phys. Lett. 467 (2008) 191.
[34] M. Anpo, H. Yamashita, K. Ikeue, Y. Fujii, S.G. Zhang, Y. Ichihashi, D.R. Park, Y. Suzuki, K. Koyano, T. Tatsumi, Catal. Today 44 (1998) 327.
[35] G.S. Thomas, P.V. Kamath, Solid State Sci. 8 (2006) 1181.
[36] Y. Izumi, T. Itoi, S. Peng, K. Oka, Y. Shibata, J. Phys. Chem. C 113 (2009) 6706.
[37] X. Gao, I.E. Wachs, J. Phys. Chem. B 104 (2000) 1261.
[38] J.A. Bearden, Rev. Mod. Phys. 39 (1967) 78.
[39] G. Zschornack, Handbook of X-ray Data, Springer, Berlin/Heidelberg, 2007.
[40] M. Vaarkamp, H. Linders, D. Koningsberger, XDAP version 2.2.7, XAFS Services International, Woudenberg, The Netherlands, 2006.
[41] N.J. Calos, J.S. Forrester, G.B. Schaffer, J. Solid State Chem. 122 (1996) 273.
[42] B.G. Hyde, S. Andersson, Inorganic Crystal Structures, Wiley, New York, 1989. p. 55.
[43] L. Ankudinov, B. Ravel, J.J. Rehr, S.D. Condradson, Phys. Rev. B 58 (1998) 7565.
[44] K.J. Hong, T.S. Jeong, J. Cryst. Growth 280 (2005) 545.
[45] Y. Izumi, K. Konishi, H. Yoshitake, Bull. Chem. Soc. Jpn. 81 (2008) 1241.
[46] Y. Sun, Y. Zhou, Z. Wang, X. Ye, Appl. Surf. Sci. 255 (2009) 6372.
[47] A. Ennadi, A. Legrouri, A. De Roy, J.P. Besse, J. Solid State Chem. 152 (2000) 568.
[48] I.H. Tseng, J.C.S. Wu, H.Y. Chou, J. Catal. 221 (2004) 432.
[49] M.A. Aramendia, Y. Aviles, J.A. Benitez, V. Borau, C. Jimenez, J.M. Marinas, J.R. Ruiz, F.J. Urbano, Micropor. Mesopor. Mater. 29 (1999) 319.
[50] Y. Izumi, Y. Shibata, Chem. Lett. 38 (2009) 912.
[51] Y. Izumi, K. Konishi, D. Obaid, T. Miyajima, H. Yoshitake, Anal. Chem. 79 (2007) 6933.
[52] D. Masih, H. Yoshitake, Y. Izumi, Appl. Catal. A 325 (2007) 276.